I&EC research
Industrial & Engineering Chemistry Research

Article

pubs.acs.org/IECR

Mathematical Modeling of a Dip-Coating Process Using Concentrated Dispersions

Juan Manuel Peralta* and Bárbara E. Meza

Instituto de Desarrollo Tecnológico para la Industria Química (INTEC), Universidad Nacional del Litoral – CONICET, Güemes 3450, S3000GLN, Santa Fe, Argentina

ABSTRACT: Industrial dip coating is a simple and easy to access technique that can be considered as a self-metered coating process. Practical applications of films obtained by this method include decorative, protective, and functional purposes. The objective of this work was to develop a 2D mathematical model of the fluid-dynamic variables of the dip-coating draining stage of a finite vertical plate, considering nonevaporative and isothermal conditions. Concentrated dispersions were considered, such as those whose rheological behavior was described by an extension of a theoretical rheological model proposed by Quemada. As a result, an analytical and simple mathematical model that relates the main fluid parameters could be obtained. The model was achieved based upon rigorous mass and momentum balances applied to the draining stage of a monophasic, isothermal, and nonevaporative system, where the highest forces are viscous and gravitational. Parameters that were estimated are the velocity profile, average velocity, flow rate, local thickness, and average thickness of the film. Finally, experimental validation was performed by using experimental data (rheological properties, densities, and average film thickness values) of several representative concentrated dispersions (emulsions and suspensions) obtained in this work and from the literature. All the information achieved in this study can be useful to control and predict the thickness and homogeneity of the film during an industrial coating process, in order to satisfy the quality requirements of the final product.

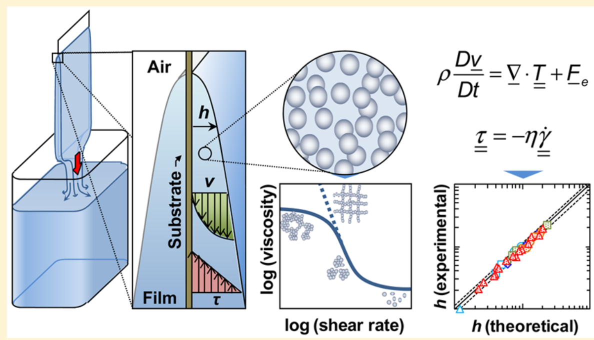

1. INTRODUCTION

The industrial dip-coating process is a simple and easy to access technique that is also considered a profitable method due to its low-cost, waste-free, and low-energy consumption characteristics.[1] Dip coating can be considered as a self-metered coating process, in which the final wet film thickness is mostly controlled by the interaction of the fluid flow with the coating applicator.[2,3] In this method, a rigid or flexible solid substrate is dipped into a reservoir containing a film-forming fluid and then it is withdrawn from the reservoir vertically (or with a certain inclination angle) at a controlled speed.[4] After that, several phenomena, such as fluid-draining by gravity, liquid layer-drying by solvent evaporation, and film-curing by chemical and/or physical reactions, may occur in order to complete the coating deposition.[5,6] Specifically, the fluid dynamics of the draining stage and its effect on the final film properties have been studied due to its technological implications and benefits.[7,8]

In food engineering, practical applications of films obtained by dip coating include decorative, protective, and functional proposes.[9−11] Because the film has to satisfy the thickness and the homogeneity requirements of the final food product, the optimum combination of substrate characteristics (geometry, porosity, etc.), environmental factors (temperature, humidity, etc.), and fluid properties (density, viscosity, etc.) is expected to be essential variables.[12,13]

However, the connection of film-forming fluid viscosity and rheological properties with coating performance is considered complicated due to difficulties in linking both phenomena.[13] In recent years, efforts have been put forth to mathematically model the transport phenomena during dip-coating processes in order to obtain mathematical expressions of several fluid-dynamic variables (such as velocity and film thickness profiles). In those studies, a mathematical model that represents the rheological behavior of the film-forming fluid has been used in the balance equations to represent in a more adequate and realistic way the flow performance.[3,14,15]

In this sense, an interesting theoretical rheological model proposed by Quemada[16] was extensively used in the literature.[17−20] The model was developed according to a structural approach for monodispersed suspensions, where dispersions of structural units are based on the concept of the effective volume fraction that depends on flow conditions. Dispersions consist of insoluble particles distributed in a continuous liquid phase, that can be called suspensions, emulsions, or foams when the particulate phase is solid, liquid, or gas with a volume fraction less than a maximum packing value.[21] According to Quemada,[16] a number of complex fluids used for industrial applications (for example, slurries, paints, coatings, concrete, foods, and cosmetics) have rheological

Received: June 1, 2016
Revised: July 29, 2016
Accepted: August 1, 2016
Published: August 1, 2016

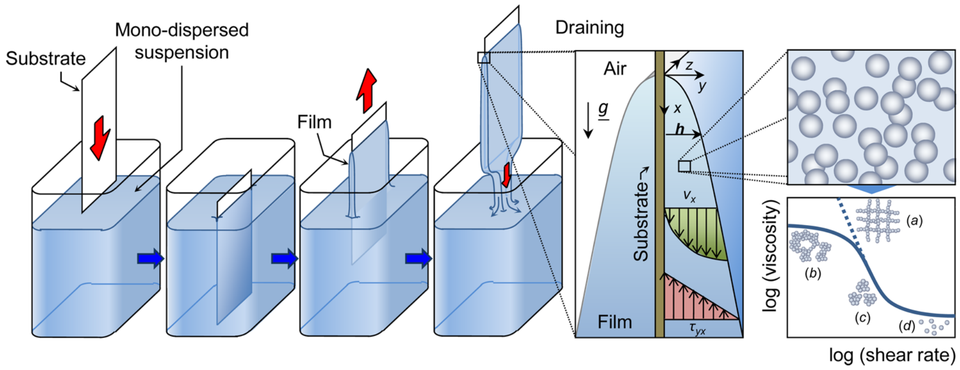

Figure 1. Schematic diagram of the dip-coating process showing the draining stage using a dispersion as a film-forming fluid. As an example, the log−log subfigure shows an adaptation of the structural interpretation of shear-thinning behavior provided by Quemada,[16] due to progressive rupturing of large clusters as the shear rate is increased: (*a*) macrostructure (network), (*b*) clusters of mesostructures, (*c*) mesostructures (small flocs), and (*d*) microstructures (small particles).

properties under steady and unsteady conditions that can approximately be described as those of concentrated dispersions of structural units.

The theoretical nature of the model proposed by Quemada allows establishing physical interpretation of its rheological parameters obtained for several materials.[17−20] By choosing conveniently the model variable values, the model yields some rheological expressions that can be found extensively in the literature (for instance, Heinz−Casson,[22] Casson,[23] and Ellis[24] models). Therefore, the Quemada equation could predict a wide spectrum of rheological behaviors, such as pseudoplastics, plastics, and dilatants phenomena.[16]

The theoretical study of the dip coating that includes the mathematical modeling with their analytical solution in a 2D system, using concentrated dispersions as film-forming fluids whose rheological behavior can be described with the expression proposed by Quemada,[16] was not found in the literature. This information can be useful to control and predict the film thickness during industrial food coating processes to decrease the need for trial-and-error predictions. Consequently, the objective of this work was to develop a mathematical model of the fluid-dynamic variables of the dip-coating draining stage of a finite vertical plate using concentrate dispersions, considering non-evaporative and isothermal conditions. The mathematical model was validated by using experimental data obtained in this work and from the literature.

2. THEORETICAL APPROACH

2.1. Equations of Change. A schematic diagram of the studied dip-coating process is shown in Figure 1. This figure shows that the present system is similar to the process that was described and analyzed in a previous work.[14,15] However, it is important to mention that, due to the nature of the constitutive model adopted later, a detailed description of the steps used to obtain the balances and the nondimensionalization process is necessary to understand the resulting expressions for the main variables. Briefly, the studied phenomena occur far away from the meniscus formed at the surface of the fluid reservoir. Then, the equations of change describing the phenomena in an isothermal and nonevaporative dip-coating process are the following:

- Total mass balance (*i.e.* continuity equation):

$$\frac{\partial \rho}{\partial t} + \underline{\nabla}\cdot(\rho \underline{v}) = 0 \tag{1}$$

- Momentum balance:

$$\rho\left(\frac{\partial \underline{v}}{\partial t} + \underline{v}\cdot\underline{\nabla}\,\underline{v}\right) = -\underline{\nabla}P - \underline{\nabla}\cdot\underline{\underline{\tau}} + \underline{F}_e \tag{2}$$

The following assumptions were considered: (1) the film-forming fluid is incompressible ($\rho \neq f(\underline{x}, t)$), (2) the external forces are mainly gravitational ($\underline{F}_e = \rho\underline{g}$), (3) the surface interactions are negligible ($Ca \to \infty$), (4) the system is open ($\nabla\underline{P} \cong 0$), (5) the system can be represented in Cartesian coordinates ($\underline{x} = \underline{e}_x x + \underline{e}_y y + \underline{e}_z z$), (6) the problem is mainly 2D (*i.e.* $v_z \cong 0$ and changes in the z-direction are negligible: $\partial/\partial z \cong 0$), and (7) gravity acts in the x-direction ($\underline{g} = \underline{e}_x g_x$),

$$\frac{\partial v_x}{\partial x} + \frac{\partial v_y}{\partial y} = 0 \tag{3}$$

$$\rho\left(\frac{\partial v_x}{\partial t} + v_x\frac{\partial v_x}{\partial x} + v_y\frac{\partial v_x}{\partial y}\right) = -\left(\frac{\partial \tau_{xx}}{\partial x} + \frac{\partial \tau_{yx}}{\partial y}\right) + \rho g_x \tag{4}$$

$$\rho\left(\frac{\partial v_y}{\partial t} + v_x\frac{\partial v_y}{\partial x} + v_y\frac{\partial v_y}{\partial y}\right) = -\left(\frac{\partial \tau_{xy}}{\partial x} + \frac{\partial \tau_{yy}}{\partial y}\right) \tag{5}$$

Due to the complexity of the system expressed by eqs 3−5, analytical solutions are difficult or impossible to obtain. Consequently, a dimensional analysis is useful in order to obtain simpler expressions to eqs 3−5 that are also representative of the phenomena taking place in the studied process. The following dimensionless variables are defined:

$$\tilde{v}_x = \frac{v_x}{U} \tag{6}$$

$$\tilde{v}_y = \frac{v_y}{V} \tag{7}$$

$$\tilde{x} = \frac{x}{L} \tag{8}$$

$$\tilde{y} = \frac{y}{h_L} \tag{9}$$

$$\tilde{\tau}_{xy} = \tilde{\tau}_{yx} = \frac{\tau_{xy}}{\eta_{ref}(U/h_L + V/L)} = \frac{\tau_{xy}}{\eta_{ref}(U/h_L)(1 + \varepsilon^2)} \tag{10}$$

DOI: 10.1021/acs.iecr.6b02107
Ind. Eng. Chem. Res. 2016, 55, 9295−9311

$$\tilde{\tau}_{xx} = \frac{\tau_{xx}}{\eta_{ref}(U/L)} \tag{11}$$

$$\tilde{\tau}_{yy} = \frac{\tau_{yy}}{\eta_{ref}(V/h_L)} \tag{12}$$

$$\tilde{t} = \frac{t}{(L/U)} \tag{13}$$

$$\varepsilon = h_L/L \tag{14}$$

where U and V are the reference velocities for the x-direction and y-direction, respectively [m s^{-1}], L is the length of the plate [m], h_L is the local thickness of the film at L [m], and η_{ref} is an apparent steady state viscosity at a reference condition. It is important to mention that the dimensionless form of the stress tensor components was chosen taking into account that[25] $\tau_{yx} = -\eta(\partial v_y/\partial x + \partial v_x/\partial y)$, $\tau_{xx} = -2\eta(\partial v_x/\partial x)$ and $\tau_{yy} = -2\eta(\partial v_y/\partial y)$.

Using the assumptions and rationale presented by Peralta et al.[14] and eqs 6−14, the components of the momentum equation (i.e., eqs 4 and 5) yield:

$$\mathrm{Re}\varepsilon\left(\frac{\partial \tilde{v}_x}{\partial \tilde{t}} + \tilde{v}_x\frac{\partial \tilde{v}_x}{\partial \tilde{x}} + \tilde{v}_y\frac{\partial \tilde{v}_x}{\partial \tilde{y}}\right) = -\left[\varepsilon\frac{\partial \tilde{\tau}_{xx}}{\partial \tilde{x}} + (\varepsilon^2+1)\frac{\partial \tilde{\tau}_{yx}}{\partial \tilde{y}}\right] + \mathrm{St} \tag{15}$$

$$\mathrm{Re}\varepsilon\left(\frac{\partial v_y}{\partial t} + v_x\frac{\partial v_y}{\partial x} + v_y\frac{\partial v_y}{\partial y}\right) = -\left[(\varepsilon^2+1)\frac{\partial \tau_{xy}}{\partial x} + \frac{\partial \tau_{yy}}{\partial y}\right] \tag{16}$$

where St = Re/Fr is the Stokes number,[26] $\mathrm{Re} = \rho U h_L/\eta_{ref}$ is the Reynolds number, and $Fr = U^2/(g_x h_L)$ is the Froude number.

Taking into account that the length of the plate is much larger than the average thickness of the film, that is $\varepsilon \ll 1$, and the flow is in the laminar regime (usually the viscosity of the coating liquid is high) so that $\mathrm{Re}\varepsilon \ll 1$, then, the set of equations that can be used to describe the flow of a coating film during the stage of unsteady draining becomes

$$\frac{\partial \tilde{v}_x}{\partial \tilde{x}} + \frac{\partial \tilde{v}_y}{\partial \tilde{y}} = 0 \tag{17}$$

$$\frac{\partial \tilde{\tau}_{yx}}{\partial \tilde{y}} \cong \mathrm{St} \tag{18}$$

$$\frac{\partial \tilde{\tau}_{xy}}{\partial \tilde{x}} + \frac{\partial \tilde{\tau}_{yy}}{\partial \tilde{y}} \cong 0 \tag{19}$$

It should be pointed out that the order of magnitude of Re and Fr have to be similar for obtaining an analytical solution different than a constant.

2.2. Range of Theoretical Validity of the Approach. An important feature of the theoretical approach presented here is to verify the range of validity of the set of eqs 17−19. The following set of conditions was assumed to be true:

$$\varepsilon \ll 1 \tag{20}$$

$$\mathrm{Re}\varepsilon \ll 1 \tag{21}$$

$$\mathrm{St} \cong O(1) \tag{22}$$

As stated by Peralta et al.,[14] it is noteworthy that in order to evaluate eqs 20−22, two parameters need to be defined: η_{ref} and U. The definition of these parameters will depend on the rheological model adopted.

2.3. Constitutive Equation for the Generalized Newtonian Fluid. To close the system proposed by eqs 17−19, an additional equation that relates the rate of deformation (expressed as a function of the velocity gradients in the material) to the stress in the film is needed. A simple way to obtain this relationship is to assume that the fluid material behaves as a generalized Newtonian fluid:[24,25]

$$\underline{\underline{\tau}} = -\eta\,\dot{\underline{\underline{\gamma}}} \tag{23}$$

where $\underline{\underline{\tau}}$ is the viscous stress tensor [Pa], $\dot{\underline{\underline{\gamma}}}$ is the rate-of-strain tensor (*i.e.* shear rate tensor) [s^{-1}], $\eta = f(|\underline{\underline{\tau}}|$ or $|\dot{\underline{\underline{\gamma}}}|, T, P, C)$ is the apparent steady state viscosity (scalar quantity) [Pa s], $|\underline{\underline{\tau}}|$ is the magnitude of $\underline{\underline{\tau}}$, $|\dot{\underline{\underline{\gamma}}}|$ is the magnitude of $\dot{\underline{\underline{\gamma}}}$ [s^{-1}], T is the temperature [K], P is the thermodynamic pressure [Pa], and C is the concentration [kg m^{-3}].

Quemada[16] proposed a well-known theoretical rheological model for η based on a structural approach for monodispersed suspensions. A generalization of their model is

$$\eta = \eta_\infty\left[\frac{1+\Gamma^p}{(\eta_\infty/\eta_0)^{1/q} + \Gamma^p}\right]^q \tag{24}$$

where Γ is a dimensionless shear variable that could be conveniently $|\underline{\underline{\tau}}|/\tau_c$ or $|\dot{\underline{\underline{\gamma}}}|/\dot{\gamma}_c$, τ_c is a characteristic shear stress [Pa], $\dot{\gamma}_c$ is a characteristic shear rate [s^{-1}], $\eta_0 = f_1(T, P, C)$ is the limiting steady state viscosity when $\Gamma \to 0$ (that is, $\eta_0 = \lim_{\Gamma\to 0}\eta$) [Pa s], $\eta_\infty = f_2(T, P, C)$ is the limiting steady state viscosity when $\Gamma \to \infty$ (that is, $\eta_\infty = \lim_{\Gamma\to\infty}\eta$) [Pa s], and $p = f_3(T, P, C)$ and $q = f_4(T, P, C)$ are dimensionless coefficients. It is important to mention that the expression proposed by Quemada[16] has $q = 2$ as a simplified version of a more general expression implicitly analyzed in their work (i.e., eq 24). For convenience and versatility, eq 24 will be used to estimate η in this study.

The model selected to estimate η in this work (eq 24) can yield several well-known rheological models found in the literature by choosing conveniently the values of η_0, η_∞, Γ, p, and q. For example: (1) **Quemada model:**[16] $q = 2$ then $\eta = \eta_\infty[1 + \Gamma^p]^2/[(\eta_\infty/\eta_0)^{1/2} + \Gamma^p]^2$; (2) **Berli−Quemada model:**[17,18] $q = 2$, $p = 1$, and $\Gamma = |\underline{\underline{\tau}}|/\tau_c$ then $\eta = \eta_\infty[1 + (|\underline{\underline{\tau}}|/\tau_c)]^2/[(\eta_\infty/\eta_0)^{1/2} + (|\underline{\underline{\tau}}|/\tau_c)]^2$; (3) **Heinz−Casson model:**[22] $q = 1/p$, $\Gamma = |\dot{\underline{\underline{\gamma}}}|/\dot{\gamma}_c$, and $\eta_0 \gg \eta_\infty$ then $\eta = \eta_\infty[1 + (|\dot{\underline{\underline{\gamma}}}|/\dot{\gamma}_c)^p]^{1/p}/[(\eta_\infty/\eta_0)^p + (|\dot{\underline{\underline{\gamma}}}|/\dot{\gamma}_c)^p]^{1/p}$; (4) **Casson model:**[23] $q = 2$, $p = {}^1/_2$, $\Gamma = |\dot{\underline{\underline{\gamma}}}|/\dot{\gamma}_c$, and $\eta_0 \gg \eta_\infty$ then $\eta = \eta_\infty[1 + (|\dot{\underline{\underline{\gamma}}}|/\dot{\gamma}_c)^{1/2}]^2/(\eta_\infty/\eta_0)^{1/2} + (|\dot{\underline{\underline{\gamma}}}|/\dot{\gamma}_c)^{1/2}]^2$; (5) **Sisko model:**[27] $q = 1$, $p = -p$, $\Gamma = |\dot{\underline{\underline{\gamma}}}|/\dot{\gamma}_c$, and $\eta_0 \gg \eta_\infty$ then $\eta = \eta_\infty + (\eta_\infty/\dot{\gamma}_c^p)|\dot{\underline{\underline{\gamma}}}|^p$; (6) **Bingham model:**[28] $q = 1$, $p = 1$, $\Gamma = |\dot{\underline{\underline{\gamma}}}|/\dot{\gamma}_c$, and $\eta_0 \gg \eta_\infty$ then $\eta = \eta_\infty + \eta_\infty\dot{\gamma}_c/|\dot{\underline{\underline{\gamma}}}|$; (7) **Cross model:**[29] $q = -1$ and $\Gamma = |\dot{\underline{\underline{\gamma}}}|/\dot{\gamma}_c$ then $\eta = \eta_\infty + (\eta_0 - \eta_\infty)/[1 + (|\dot{\underline{\underline{\gamma}}}|/\dot{\gamma}_c)^p]$; (8) **Meter−Bird model:**[30] $q = -1$ and $\Gamma = |\underline{\underline{\tau}}|/\tau_c$ then $\eta = \eta_\infty + (\eta_0 - \eta_\infty)/[1 + (|\underline{\underline{\tau}}|/\tau_c)^p]$; (9) **Reiner−Phillipoff model:**[24] $q = -1$, $p = 2$, and $\Gamma = |\underline{\underline{\tau}}|/\tau_c$ then $\eta = \eta_\infty + (\eta_0 - \eta_\infty)/[1 + (|\underline{\underline{\tau}}|/\tau_c)^2]$; (10) **Peek−Mclean−Williamson model:**[31] $q = -1$, $p = 1$, and $\Gamma = |\underline{\underline{\tau}}|/\tau_c$ then $\eta = \eta_\infty + (\eta_0 - \eta_\infty)/[1 + (|\underline{\underline{\tau}}|/\tau_c)]$; (11) **Ellis model:**[24] $q = -1$, Γ

DOI: 10.1021/acs.iecr.6b02107
Ind. Eng. Chem. Res. 2016, 55, 9295−9311

$= |\underline{\underline{\tau}}|/\tau_c$, and $\eta_0 \gg \eta_\infty$ then $\eta = \eta_0/[1 + (|\underline{\underline{\tau}}|/\tau_c)^p]$; (12)
Newtonian model: $\eta_0 = \eta_\infty$ then $\eta = \mu$.

2.4. Velocity Profile within the Film. The first step to obtain the velocity profile of the film described by eq 24, and the rest of the parameters studied in this work, is to express the functionality of Γ (i.e., $|\underline{\underline{\tau}}|/\tau_c$ or $|\dot{\underline{\underline{\gamma}}}|/\dot{\gamma}_c$) in terms of system variables and parameters. The correct derivation of these functionalities is essential for a rigorous treatment of the problem. Both quantities, $|\underline{\underline{\tau}}|$ and $|\dot{\underline{\underline{\gamma}}}|$ can be defined in terms of its respective magnitudes as[25]

$$|\underline{\underline{\tau}}| = \sqrt{\frac{1}{2}(\underline{\underline{\tau}}:\underline{\underline{\tau}})} = \sqrt{\frac{1}{2}\sum_i \sum_j \tau_{ij}\tau_{ji}} \quad (25)$$

$$|\dot{\underline{\underline{\gamma}}}| = \sqrt{\frac{1}{2}(\dot{\underline{\underline{\gamma}}}:\dot{\underline{\underline{\gamma}}})} = \sqrt{\frac{1}{2}\sum_i \sum_j \dot{\gamma}_{ij}\dot{\gamma}_{ji}} \quad (26)$$

where $\dot{\underline{\underline{\gamma}}} = \nabla \underline{v} + (\nabla \underline{v})^T$ and $\dot{\gamma}_{ij} = \partial v_i/\partial x_j + \partial v_j/\partial x_i$.

Considering the symmetric nature of $\underline{\underline{\tau}}$ (*i.e.* $\tau_{ij} = \tau_{ji}$) and the fact that the system can be described as a Cartesian 2D system, eqs 25 and 26 can be written as

$$|\underline{\underline{\tau}}| = \sqrt{\frac{1}{2}(\tau_{xx}^2 + \tau_{yy}^2) + \tau_{xy}^2} \quad (27)$$

$$|\dot{\underline{\underline{\gamma}}}| = \sqrt{2\left[\left(\frac{\partial v_x}{\partial x_x}\right)^2 + \left(\frac{\partial v_y}{\partial x_y}\right)^2\right] + \left(\frac{\partial v_x}{\partial x_y} + \frac{\partial v_y}{\partial x_x}\right)^2} \quad (28)$$

At this time, a dimensional analysis is necessary to obtain convenient expressions of eqs 25 and 26. Using eqs 6–14 in eqs 27 and 28:

$$|\underline{\underline{\tilde{\tau}}}| = \sqrt{\frac{\varepsilon^2}{2}(\tilde{\tau}_{xx}^2 + \tilde{\tau}_{yy}^2) + (1+\varepsilon^2)^2\tilde{\tau}_{xy}^2} \quad (29)$$

$$|\underline{\underline{\tilde{\dot{\gamma}}}}| = \sqrt{2\varepsilon^2\left[\left(\frac{\partial \tilde{v}_x}{\partial \tilde{x}}\right)^2 + \left(\frac{\partial \tilde{v}_y}{\partial \tilde{y}}\right)^2\right] + \left(\frac{\partial \tilde{v}_x}{\partial \tilde{y}} + \varepsilon^2\frac{\partial \tilde{v}_y}{\partial \tilde{x}}\right)^2} \quad (30)$$

where $|\underline{\underline{\tilde{\tau}}}| = |\underline{\underline{\tau}}|/[\eta_{ref}(U/h_L)]$ and $|\underline{\underline{\tilde{\dot{\gamma}}}}| = |\dot{\underline{\underline{\gamma}}}|/(U/h_L)$.

According to eq 18, τ_{yx} is the unique component in $\underline{\underline{\tau}}$ that is necessary to calculate. Therefore, considering that[25]

$$\tau_{yx} = -\eta\left(\frac{\partial v_y}{\partial x} + \frac{\partial v_x}{\partial y}\right) \quad (31)$$

Equations 6–10 were used to nondimensionalize eq 31:

$$\tilde{\tau}_{yx} = -\tilde{\eta}\left(\varepsilon^2\frac{\partial \tilde{v}_y}{\partial \tilde{x}} + \frac{\partial \tilde{v}_x}{\partial \tilde{y}}\right) \quad (32)$$

where $\tilde{\eta} = \eta/\eta_{ref}$.

Regarding that $\varepsilon \ll 1$ and $\varepsilon^2 \ll 1$, eqs 29, 30, and 32 yield, respectively:

$$|\underline{\underline{\tilde{\tau}}}| \cong |\tilde{\tau}_{xy}| = \tilde{\tau}_{xy} = \tilde{\tau} \quad (33)$$

$$|\underline{\underline{\tilde{\dot{\gamma}}}}| \cong \left|\frac{\partial \tilde{v}_x}{\partial \tilde{y}}\right| = \tilde{\dot{\gamma}} \quad (34)$$

$$\tilde{\tau}_{yx} \cong -\tilde{\eta}\frac{\partial \tilde{v}_x}{\partial \tilde{y}} \quad (35)$$

Now, integrating eq 18:

$$\tilde{\tau}_{yx} \cong \mathrm{St}\tilde{y} + C_1 \quad (36)$$

Taking into account that the film will be surrounded at the top by air and that $\eta_{air} \ll \eta_{film}$, a feasible boundary condition will be $\tilde{\tau}_{yx} \cong 0$ in $\tilde{y} \cong \tilde{h}(\tilde{x})$, where $\tilde{h}(\tilde{x}) = h(x)/h_L$. Thus, eq 36 yields

$$\tilde{\tau}_{yx} \cong -\mathrm{St}(\tilde{h} - \tilde{y}) \quad (37)$$

This equation predicts a linear profile of the shear stress across the film with a slope that depends on the ratio between gravitational and viscous forces. The nature of eq 37 shows that it is independent of the type of the coating material (*i.e.* Newtonian, viscoelastic, etc.), and the maximum shear stress is expected at the plate surface: $\tilde{\tau}_m \cong -\mathrm{St}\tilde{h}$.

Now, using previous definitions, the dimensionless forms of eq 24 are

$$\tilde{\eta} = \tilde{\eta}_\infty\left[\frac{1 + (|\underline{\underline{\tilde{\tau}}}|/\tilde{\tau}_c)^p}{(\tilde{\eta}_\infty/\tilde{\eta}_0)^{1/q} + (|\underline{\underline{\tilde{\tau}}}|/\tilde{\tau}_c)^p}\right]^q \quad (38)$$

$$\tilde{\eta} = \tilde{\eta}_\infty\left[\frac{1 + (|\underline{\underline{\tilde{\dot{\gamma}}}}|/\tilde{\dot{\gamma}}_c)^p}{(\tilde{\eta}_\infty/\tilde{\eta}_0)^{1/q} + (|\underline{\underline{\tilde{\dot{\gamma}}}}|/\tilde{\dot{\gamma}}_c)^p}\right]^q \quad (39)$$

where $\tilde{\tau}_c = \tau_c/[\eta_{ref}(U/h_L)]$ and $\tilde{\dot{\gamma}}_c = \dot{\gamma}_c/(U/h_L)$.

It is important to mention that, as stated by Quemada,[16] although the same symbols were adopted for the dimensionless parameters p and q in eqs 38 and 39, different values are expected for those parameters when $\Gamma = |\underline{\underline{\tilde{\tau}}}|/\tilde{\tau}_c$ or $\Gamma = |\underline{\underline{\tilde{\dot{\gamma}}}}|/\tilde{\dot{\gamma}}_c$. Also, to simplify the presentation of the equations, henceforth, approximately equal signs will be replaced by equal signs, and the simplification in notation resulting from eqs 33 and 34 (in dimensional and nondimensional forms) will be used when necessary.

2.4.1. Velocity Profile for $\eta = \eta(\tau)$. Using eqs 33 and 35, and regarding eq 37 to change variables, the velocity profile based on momentum balance can be written as

$$\tilde{v}_x = -\frac{1}{\mathrm{St}}\int_{\tilde{\tau}_m}^{\tilde{\tau}} \frac{\tilde{\tau}}{\tilde{\eta}} d\tilde{\tau} \quad (40)$$

Replacing eq 38 into eq 40 and defining a normalized and dimensionless shear stress parameter $Z_S = (\tilde{\tau}/\tilde{\tau}_c)^p/[1 + (\tilde{\tau}/\tilde{\tau}_c)^p]$, then:

$$\tilde{v}_x = -\frac{\tilde{\tau}_c^2(-1)^{-2/p-1}[1 - (\tilde{\eta}_\infty/\tilde{\eta}_0)^{1/q}]^q}{\mathrm{St}\tilde{\eta}_\infty p} \times \int_{Z_{S,m}}^{Z_S} Z_S^{2/p-1}(-1 + Z_S)^{-2/p-1} \times \left[\frac{1}{(\tilde{\eta}_\infty/\tilde{\eta}_0)^{-1/q} - 1} + Z_S\right]^q dZ_S \quad (41)$$

where $Z_{S,m} = (\tilde{\tau}_m/\tilde{\tau}_c)^p/[1 + (\tilde{\tau}_m/\tilde{\tau}_c)^p]$.

Now, to integrate eq 41 and considering some of the work presented by Srivastava and Hussain,[32] the following expression will be used:

DOI: 10.1021/acs.iecr.6b02107
Ind. Eng. Chem. Res. 2016, 55, 9295−9311

$$\int_0^Z Z^{r-1}(a+Z)^c(b+Z)^d dZ = \frac{a^c b^d}{r} Z^r F_1\left(r; -c, -d; r+1; -\frac{Z}{a}, -\frac{Z}{b}\right) \quad (42)$$

where $F_1(\alpha; \beta, \gamma; \delta; z_1, z_2)$ is the Appell hypergeometric function of the first kind and eq 42 holds when $\min\{\mathbb{R}(r), \mathbb{R}(1)\} > 0$; $\max\{|Z/a|, |Z/b|\} > 1$; $Z \neq 0$. It is important to mention that the Appell hypergeometric functions are special cases of the Lauricella hypergeometric functions and general cases of the Gauss hypergeometric functions.[32]

Using eq 42 in eq 41, the velocity profile can be estimated as

$$\tilde{v}_x = \frac{\tilde{\tau}_c^2}{2\mathrm{St}\tilde{\eta}_0}[\psi(0) - \psi(\tilde{y})] \quad (43)$$

$$\psi(0) = Z_{\mathrm{S,m}}^{2/p} F_1\left(\frac{2}{p}; \frac{2}{p}+1, -q; \frac{2}{p}+1; Z_{\mathrm{S,m}}, \eta_c Z_{\mathrm{S,m}}\right) \quad (44)$$

$$\psi(\tilde{y}) = Z_{\mathrm{S}}^{2/p} F_1\left(\frac{2}{p}; \frac{2}{p}+1, -q; \frac{2}{p}+1; Z_{\mathrm{S}}, \eta_c Z_{\mathrm{S}}\right) \quad (45)$$

$$Z_{\mathrm{S,m}} = (\tilde{\tau}_{\mathrm{m}}/\tilde{\tau}_c)^p/[1 + (\tilde{\tau}_{\mathrm{m}}/\tilde{\tau}_c)^p] = (\mathrm{St}\tilde{h}/\tilde{\tau}_c)^p /[1 + (\mathrm{St}\tilde{h}/\tilde{\tau}_c)^p] \quad (46)$$

$$Z_{\mathrm{S}} = (\tilde{\tau}/\tilde{\tau}_c)^p/[1 + (\tilde{\tau}/\tilde{\tau}_c)^p] = [\mathrm{St}(\tilde{h} - \tilde{y})/\tilde{\tau}_c]^p /\{1 + [\mathrm{St}(\tilde{h} - \tilde{y})/\tilde{\tau}_c]^p\} \quad (47)$$

$$\eta_c = 1 - (\tilde{\eta}_\infty/\tilde{\eta}_0)^{-1/q} \quad (48)$$

2.4.2. Velocity Profile for $\eta = \eta(\dot{\gamma})$. The velocity profile as a function of the shear rate can be estimated using eqs 34 and 35:

$$\tilde{v}_x = \int_{\tilde{\dot{\gamma}}_{\mathrm{m}}}^{\tilde{\dot{\gamma}}} \frac{\tilde{\dot{\gamma}}}{(\partial\tilde{\dot{\gamma}}/\partial\tilde{y})} d\tilde{\dot{\gamma}} = -\frac{1}{\mathrm{St}} \int_{\tilde{\dot{\gamma}}_{\mathrm{m}}}^{\tilde{\dot{\gamma}}} \left[\tilde{\dot{\gamma}}\tilde{\eta} + \tilde{\dot{\gamma}}^2 \frac{\partial\tilde{\eta}}{\partial\tilde{\dot{\gamma}}}\right] d\tilde{\dot{\gamma}} \quad (49)$$

where $\tilde{\dot{\gamma}}_{\mathrm{m}} = |\partial\tilde{v}_x/\partial\tilde{y}|_{\tilde{y}=0}$. Defining a normalized and dimensionless shear rate parameter $Z_{\mathrm{R}} = (\tilde{\dot{\gamma}}/\tilde{\dot{\gamma}}_c)^p/[1 + (\tilde{\dot{\gamma}}/\tilde{\dot{\gamma}}_c)^p]$ to change variables in eq 49:

$$\begin{aligned}\tilde{v}_x = -\frac{\tilde{\eta}_\infty \tilde{\dot{\gamma}}_c^2 (-1)^{-2/p-1}}{\mathrm{St}p[1 - (\tilde{\eta}_\infty/\tilde{\eta}_0)^{1/q}]^q} \Bigg\{ &\int_{Z_{\mathrm{R,m}}}^{Z_{\mathrm{R}}} Z_{\mathrm{R}}^{2/p-1}(-1 + Z_{\mathrm{R}})^{-2/p-1} \times \left[\frac{1}{(\tilde{\eta}_\infty/\tilde{\eta}_0)^{-1/q} - 1} + Z_{\mathrm{R}}\right]^{-q} dZ_{\mathrm{R}} \\ &+ qp \int_{Z_{\mathrm{R,m}}}^{Z_{\mathrm{R}}} Z_{\mathrm{R}}^{2/p}(-1 + Z_{\mathrm{R}})^{-2/p} \times \left[\frac{1}{(\tilde{\eta}_\infty/\tilde{\eta}_0)^{-1/q} - 1} + Z_{\mathrm{R}}\right]^{-1-q} dZ_{\mathrm{R}} \Bigg\}\end{aligned} \quad (50)$$

Using eq 42 to solve eq 50 and obtaining a convenient form of its solution:

$$\tilde{v}_x = \frac{\tilde{\eta}_0 \tilde{\dot{\gamma}}_c^2}{2\mathrm{St}}[\psi(0) - \psi(\tilde{y})] \quad (51)$$

$$\begin{aligned}\psi(0) = {}& Z_{\mathrm{R,m}}^{2/p} F_1\left(\frac{2}{p}; \frac{2}{p}+1, q; \frac{2}{p}+1; Z_{\mathrm{R,m}}, \eta_c Z_{\mathrm{R,m}}\right) \\ &+ \frac{2q\eta_c p}{(2+p)} Z_{\mathrm{R,m}}^{2/p+1} F_1\left(\frac{2}{p}+1; \frac{2}{p}, 1 + q; \frac{2}{p}+2; Z_{\mathrm{R,m}}, \eta_c Z_{\mathrm{R,m}}\right)\end{aligned} \quad (52)$$

$$\begin{aligned}\psi(\tilde{y}) = {}& Z_{\mathrm{R}}^{2/p} F_1\left(\frac{2}{p}, \frac{2}{p}+1, q; \frac{2}{p}+1; Z_{\mathrm{R}}, \eta_c Z_{\mathrm{R}}\right) \\ &+ \frac{2q\eta_c p}{(2+p)} Z_{\mathrm{R}}^{2/p+1} F_1\left(\frac{2}{p}+1; \frac{2}{p}, 1 + q; \frac{2}{p}+2; Z_{\mathrm{R}}, \eta_c Z_{\mathrm{R}}\right)\end{aligned} \quad (53)$$

$$Z_{\mathrm{R,m}} = (\tilde{\dot{\gamma}}_{\mathrm{m}}/\tilde{\dot{\gamma}}_c)^p/[1 + (\tilde{\dot{\gamma}}_{\mathrm{m}}/\tilde{\dot{\gamma}}_c)^p] \quad (54)$$

$$Z_{\mathrm{R}} = (\tilde{\dot{\gamma}}/\tilde{\dot{\gamma}}_c)^p/[1 + (\tilde{\dot{\gamma}}/\tilde{\dot{\gamma}}_c)^p] \quad (55)$$

where η_c is defined in eq 48.

It is important to mention that, for $\eta = \eta(\dot{\gamma})$, the velocity profile is estimated by using parametric equations that relate the velocity with the position perpendicular to the surface. That is, the relation between $\tilde{y}$ and $\tilde{\dot{\gamma}}$ is obtained by combining eqs 34, 35, 37, and 39:

$$\tilde{y} = \tilde{h} - \frac{\tilde{\eta}_\infty \tilde{\dot{\gamma}}}{\mathrm{St}} \left[\frac{1 + (\tilde{\dot{\gamma}}/\tilde{\dot{\gamma}}_c)^p}{(\tilde{\eta}_\infty/\tilde{\eta}_0)^{1/q} + (\tilde{\dot{\gamma}}/\tilde{\dot{\gamma}}_c)^p}\right]^q \quad (56)$$

$$\frac{\mathrm{St}\tilde{h}}{\tilde{\eta}_\infty} \tilde{\dot{\gamma}}_{\mathrm{m}}^{-1/q} = \frac{1 + (\tilde{\dot{\gamma}}_{\mathrm{m}}/\tilde{\dot{\gamma}}_c)^p}{(\tilde{\eta}_\infty/\tilde{\eta}_0)^{1/q} + (\tilde{\dot{\gamma}}_{\mathrm{m}}/\tilde{\dot{\gamma}}_c)^p} \quad (57)$$

2.5. Flow Rate. The flow rate in the thickness $\tilde{h}$ can be estimated by

$$\tilde{Q} = \langle \tilde{v}_x \rangle_y \tilde{h} = \int_0^{\tilde{h}} \tilde{v}_x d\tilde{y} \quad (58)$$

where $\tilde{Q} = Q/(Uh_L)$, Q is the flow rate per unit of plate width [m^2], and $\langle \tilde{v}_x \rangle_y$ is the area-averaged velocity [m s^{-1}].

2.5.1. Flow Rate for $\eta = \eta(\tau)$. Taking into account eq 47, eq 58 can be rewritten as

$$\tilde{Q} = \frac{\tilde{\tau}_c}{\mathrm{St}p} \int_0^{Z_{\mathrm{S,m}}} \tilde{v}_x Z_{\mathrm{S}}^{1/p-1}(1 - Z_{\mathrm{S}})^{-1/p-1} dZ_{\mathrm{S}} \quad (59)$$

Now, using eqs 42 and 43−48 in eq 59, the expression for the flow rate is

$$\tilde{Q} = \frac{\tilde{\tau}_m^3}{3\mathrm{St}^2\tilde{\eta}_0}(1 - Z_{\mathrm{S,m}})^{3/p} \times F_1\left(\frac{3}{p}; \frac{3}{p}+1, -q; \frac{3}{p}+1; Z_{\mathrm{S,m}}, \eta_c Z_{\mathrm{S,m}}\right) \quad (60)$$

From eq 60 the average velocity profile can be estimated as

DOI: 10.1021/acs.iecr.6b02107
Ind. Eng. Chem. Res. 2016, 55, 9295−9311

$$\langle\tilde{v}_x\rangle_y = \frac{\tilde{\tau}_m^3\tilde{h}}{3\mathrm{St}^2\tilde{\eta}_0}(1 - Z_{\mathrm{S,m}})^{3/p} \times F_1\left(\frac{3}{p}; \frac{3}{p} + 1, -q; \frac{3}{p} + 1; Z_{\mathrm{S,m}}, \eta_c Z_{\mathrm{S,m}}\right) \quad (61)$$

and the ratio of the average velocity profile to the maximum velocity is given by

$$\frac{\langle\tilde{v}_x\rangle_y}{\tilde{v}_x|_{y=h}} = \frac{2\tilde{\tau}_m\tilde{h}}{3\mathrm{St}}(1 - Z_{\mathrm{S,m}})^{1/p} \times \frac{F_1\left(\frac{3}{p}; \frac{3}{p} + 1, -q; \frac{3}{p} + 1; Z_{\mathrm{S,m}}, \eta_c Z_{\mathrm{S,m}}\right)}{F_1\left(\frac{2}{p}; \frac{2}{p} + 1, -q; \frac{2}{p} + 1; Z_{\mathrm{S,m}}, \eta_c Z_{\mathrm{S,m}}\right)} \quad (62)$$

2.5.2. Flow Rate for $\eta = \eta(\dot{\gamma})$. Using eq 34 in eq 58 to change variables and considering eq 55:

$$\tilde{Q} = \frac{\tilde{\eta}_\infty\tilde{\dot{\gamma}}_c}{\mathrm{St}[(\tilde{\eta}_\infty/\tilde{\eta}_0)^{1/q} - 1]^q}\int_0^{Z_{\mathrm{R,m}}} \tilde{v}_x\left[qZ_{\mathrm{R}}^{1/p}(1 - Z_{\mathrm{R}})^{-1/p}(\eta_c^{-1} - Z_{\mathrm{R}})^{-q-1} + \frac{1}{p}Z_{\mathrm{R}}^{1/p-1}(1 - Z_{\mathrm{R}})^{-1/p-1}(\eta_c^{-1} - Z_{\mathrm{R}})^{-q}\right]dZ \quad (63)$$

Taking into account eqs 42 and 51−55 in eq 63, the expression for the flow rate is

$$\tilde{Q} = \frac{\tilde{\eta}_0^2\tilde{\dot{\gamma}}_{\mathrm{m}}^3}{\mathrm{St}^2}\left[\frac{q\eta_c p}{(3 + p)}Z_{\mathrm{R,m}}(1 - Z_{\mathrm{R,m}})^{3/p} \times F_1\left(\frac{3}{p} + 1; \frac{3}{p}, 1 + 2q; \frac{3}{p} + 2; Z_{\mathrm{R,m}}, \eta_c Z_{\mathrm{R,m}}\right) + \frac{2}{p^2}(1 - Z_{\mathrm{R,m}})^{3/p}F_1\left(\frac{3}{p}; \frac{3}{p} + 1, 2q; \frac{3}{p} + 1; Z_{\mathrm{R,m}}, \eta_c Z_{\mathrm{R,m}}\right)\right] \quad (64)$$

Now, from eq 64, the average velocity profile can be estimated as

$$\langle\tilde{v}_x\rangle_y = \frac{\tilde{\eta}_0^2\tilde{\dot{\gamma}}_{\mathrm{m}}^3\tilde{h}}{\mathrm{St}^2}\left[\frac{q\eta_c p}{(3 + p)}Z_{\mathrm{R,m}}(1 - Z_{\mathrm{R,m}})^{3/p} \times F_1\left(\frac{3}{p} + 1; \frac{3}{p}, 1 + 2q; \frac{3}{p} + 2; Z_{\mathrm{R,m}}, \eta_c Z_{\mathrm{R,m}}\right) + \frac{2}{p^2}(1 - Z_{\mathrm{R,m}})^{3/p}F_1\left(\frac{3}{p}; \frac{3}{p} + 1, 2q; \frac{3}{p} + 1; Z_{\mathrm{R,m}}, \eta_c Z_{\mathrm{R,m}}\right)\right] \quad (65)$$

and the ratio of the average velocity profile to the maximum velocity is given by

$$\frac{\langle\tilde{v}_x\rangle_y}{\tilde{v}_x|_{y=h}} = \frac{2\tilde{\eta}_0\tilde{\dot{\gamma}}_{\mathrm{m}}\tilde{h}}{\mathrm{St}}\left[\frac{2}{p^2}(1 - Z_{\mathrm{R,m}})^{3/p} \times F_1\left(\frac{3}{p}; \frac{3}{p} + 1, 2q; \frac{3}{p} + 1; Z_{\mathrm{R,m}}, \eta_c Z_{\mathrm{R,m}}\right) + \frac{q\eta_c p}{(3 + p)}Z_{\mathrm{R,m}}(1 - Z_{\mathrm{R,m}})^{3/p} \times F_1\left(\frac{3}{p} + 1; \frac{3}{p}, 1 + 2q; \frac{3}{p} + 2; Z_{\mathrm{R,m}}, \eta_c Z_{\mathrm{R,m}}\right)\right] \Big/ \left[(1 - Z_{\mathrm{R,m}})^{2/p}F_1\left(\frac{2}{p}; \frac{2}{p} + 1, q; \frac{2}{p} + 1; Z_{\mathrm{R,m}}, \eta_c Z_{\mathrm{R,m}}\right) + \frac{2q\eta_c p}{(2 + p)}Z_{\mathrm{R,m}}(1 - Z_{\mathrm{R,m}})^{2/p} \times F_1\left(\frac{2}{p} + 1; \frac{2}{p}, 1 + q; \frac{2}{p} + 2; Z_{\mathrm{R,m}}, \eta_c Z_{\mathrm{R,m}}\right)\right] \quad (66)$$

2.6. Estimation of the Film Thickness.

A mass balance of the film will be used to obtain the local film thickness:[14]

$$\frac{\partial\tilde{h}}{\partial\tilde{t}} + \frac{\partial\tilde{Q}}{\partial\tilde{x}} = 0 \quad (67)$$

where the quantity that is differentiated with respect to $\tilde{x}$ is the volumetric flow per unit width. Regarding $\tilde{h}(\tilde{t}, 0) = 0$ (the contact line is pinned), the solution of eq 67 as shown by Peralta et al.[14] is

$$\frac{\tilde{x}}{\tilde{t}} = \frac{\partial\tilde{Q}}{\partial\tilde{h}} \quad (68)$$

Now, applying the derivative of eq 68 into eqs 60 and 64, the expressions for the local film thickness are as follows:

When $\eta = \eta(\tau)$:

$$\left[\frac{\mathrm{St}^{qp+1}}{\tilde{\eta}_\infty\tilde{\tau}_c^{qp}(\tilde{x}/\tilde{t})}\right]^{1/q}\tilde{h}^{p+2/q} + \left[\frac{\mathrm{St}}{\tilde{\eta}_0(\tilde{x}/\tilde{t})}\right]^{1/q}\tilde{h}^{2/q} - \left(\frac{\mathrm{St}}{\tilde{\tau}_c}\right)^p\tilde{h}^p - 1 = 0 \quad (69)$$

When $\eta = \eta(\dot{\gamma})$:

$$\left[\frac{\tilde{\dot{\gamma}}_c^{qp}\mathrm{St}}{\tilde{\eta}_0(\tilde{x}/\tilde{t})^{qp+1}}\right]^{1/q}\tilde{h}^{p+2/q} + \left[\frac{\mathrm{St}}{\tilde{\eta}_\infty(\tilde{x}/\tilde{t})}\right]^{1/q}\tilde{h}^{2/q} - \left[\frac{\tilde{\dot{\gamma}}_c}{(\tilde{x}/\tilde{t})}\right]^p\tilde{h}^p - 1 = 0 \quad (70)$$

2.7. Estimation of the Average Thickness.

As stated by Peralta et al.,[14] the uniformity of the film is one of the main properties to be evaluated. This quantity can be estimated by the ratio of the average thickness to the local thickness.[33] The average dimensionless film thickness at a distance $\tilde{x}$ is defined by

$$\langle\tilde{h}\rangle_x = \frac{1}{\tilde{x}}\int_0^{\tilde{x}}\tilde{h}d\tilde{x} \quad (71)$$

where $\langle\tilde{h}\rangle_x = \langle h\rangle_x/h_L$.

To integrate eq 71 and solve the problem of the implicit nature of eqs 69 and 70 in terms of $\tilde{h}$, the method presented by Gutfinger and Tallmadge[33] will be used.

When $\eta = \eta(\tau)$:

DOI: 10.1021/acs.iecr.6b02107
Ind. Eng. Chem. Res. 2016, 55, 9295−9311

Table 1. Physical Properties of Film-Forming Fluids and Model Parameters Fitted to a Dimensional Form of Eq 38 Using Data Obtained in This Work and from the Literature

Film-forming fluid	T [°C]	C [%]	$\dot{\gamma}$ [s^{-1}]	τ [Pa]	ρ [kg m^{-3}]	ref	η_0 [Pa s]	η_∞ [Pa s]	τ_c [Pa]	p [-]	q[g] [-]	MAPE [%]
Cream[a]	20		0.2−5.4	7.7−18.6	986 ± 15[e]	f	175.79	3.22	11.06	5.89	2	7.44
Condensed milk[a]	20		0.2−3.0	1.4−17.5	1367 ± 17[e]	f	27.94	3.30	3.03	0.30	2	0.24
Microparticulated whey protein suspension[a]	20	30	0.4−192.0	0.1−11.4	1088 ± 17[e]	f	0.47	0.01	33.63	0.50	2	1.58
Glaze suspension[a]	20		0.6−13.0	30.0−202.0	1336	[35]	200.00	2.50	600.00	0.65	2	4.65
	30		0.6−50.0	14.0−255.0	1334	[35]	100.00	1.10	451.52	0.65	2	4.86
	40		0.6−50.0	9.9−162.0	1331	[35]	81.40	0.91	191.31	0.57	2	2.62
	50		0.6−50.0	4.8−108.0	1327	[35]	80.00	0.90	30.00	0.55	2	8.08
Milk chocolate + Lecithin	20	0[b]	1.9−50.0	50.9−332.9	1216	[9]	230.33	5.48	76.72	1.35	2	1.20
	20	0.1[b]	1.9−50.0	22.2−195.5	1216	[9]	119.23	3.81	21.66	1.43	2	1.52
	20	0.2[b]	1.9−50.0	16.3−160.2	1216	[9]	84.45	3.06	15.14	1.53	2	1.62
	20	0.3[b]	1.9−50.0	15.4−124.9	1216	[9]	69.49	2.42	16.29	1.68	2	2.95
	20	0.4[b]	1.9−50.0	15.6−127.4	1216	[9]	69.49	2.42	16.29	1.69	2	2.79
	20	0.5[b]	1.9−50.0	15.4−124.7	1216	[9]	69.49	2.42	16.29	1.69	2	3.20
Milk chocolate + Polyglycerol	20	0[c]	1.9−50.0	52.3−332.4	1216	[9]	228.43	5.15	82.07	1.27	2	1.26
	20	0.1[c]	1.9−50.0	31.4−296.8	1216	[9]	160.00	5.10	32.46	1.10	2	3.60
	20	0.2[c]	1.9−50.0	17.2−247.9	1216	[9]	103.87	4.97	7.99	0.97	2	1.75
	20	0.3[c]	1.9−50.0	12.4−229.4	1216	[9]	72.00	4.50	3.31	0.85	2	2.35
	20	0.4[c]	1.9−50.0	9.8−218.9	1216	[9]	50.00	4.40	0.76	0.76	2	1.50
	20	0.5[c]	1.9−50.0	8.4−240.8	1216	[9]	40.50	4.14	0.09	0.76	2	0.81
Batter Dorothy Dawson	20	50[d]	0.1−50.0	2.3−81.3	1160	[10]	135.92	0.18	507.53	0.46	2	0.52
Batter Drakes	20	50[d]	0.1−50.0	2.1−78.3	1140	[10]	136.55	0.20	375.07	0.45	2	0.60
Batter Golden Dipt	20	50[d]	0.1−50.0	14.8−463.5	1160	[10]	300.00	2.50	583.11	0.65	2	1.40
Batter Kikkoman tempura	20	50[d]	0.1−50.0	6.9−119.3	1140	[10]	173.52	1.56	157.76	0.68	2	0.88
Batter Tung−I tempura	20	50[d]	0.1−50.0	9.4−196.3	1150	[10]	213.42	2.73	254.26	0.61	2	0.75
Batter Newly Wed tempura	20	50[d]	0.1−50.0	5.4−72.7	1110	[10]	167.76	0.73	123.04	0.74	2	0.88

[a]Experiments were carried out in triplicate, showing the parameters of eq 38 (dimensional) fitted to one of these repetitions. [b]Concentration of lecithin (w/w). [c]Concentration of polyglycerol (w/w). [d]Concentration of solids (w/w). [e]Average ± standard deviation. [f]This work. [g]Fittings were carried out setting $q = 2$ for computational convenience.

$$\frac{\langle \tilde{h} \rangle_x}{\tilde{h}} = 1 - \frac{\tilde{\eta}_m}{\tilde{\tau}_m^3} \int_0^{\tilde{\tau}_m} \frac{\tilde{\tau}_m^2}{\tilde{\eta}_m} d\tilde{\tau}_m \tag{72}$$

then:

$$\frac{\langle \tilde{h} \rangle_x}{\tilde{h}} = 1 - \frac{1}{3} \frac{(1 - Z_{S,m})^{3/p}}{(1 - \eta_c Z_{S,m})^q} \times F_1\left(\frac{3}{p}; \frac{3}{p} + 1, -q; \frac{3}{p} + 1; Z_{S,m}, \eta_c Z_{S,m}\right) \tag{73}$$

where $Z_{S,m}$ is defined by eq 46.

When $\eta = \eta(\dot{\gamma})$:

$$\frac{\langle \tilde{h} \rangle_x}{\tilde{h}} = 1 - \frac{1}{\tilde{\eta}_m^2 \tilde{\dot{\gamma}}_m^3} \int_0^{\tilde{\dot{\gamma}}_m} \left(\tilde{\eta}_m \tilde{\dot{\gamma}}_m^3 \frac{\partial \tilde{\eta}_m}{\partial \tilde{\dot{\gamma}}_m} + \tilde{\eta}_m^2 \tilde{\dot{\gamma}}_m^2 \right) d\tilde{\dot{\gamma}}_m \tag{74}$$

then:

$$\frac{\langle \tilde{h} \rangle_x}{\tilde{h}} = 1 - (1 - Z_{R,m})^{3/p} (1 - \eta_c Z_{R,m})^{2q} \left[\frac{q \eta_c p}{(3 + p)} Z_{R,m} \times F_1\left(\frac{3}{p} + 1; \frac{3}{p}, 2q + 1; \frac{3}{p} + 2; Z_{R,m}, \eta_c Z_{R,m}\right) + \frac{1}{3} F_1\left(\frac{3}{p}; \frac{3}{p} + 1, 2q; \frac{3}{p} + 1; Z_{R,m}, \eta_c Z_{R,m}\right) \right] \tag{75}$$

where $Z_{R,m}$ is defined by eq 54.

2.8. Experimental Validation. The mathematical model developed in this work was validated by using experimental data (rheological properties, densities, and average film thickness values) of several representative concentrated dispersions as film-forming fluids (emulsions and suspensions) obtained in this work and from the literature.

2.8.1. Experimental Data Obtained in This Work. Commercial pasteurized milk cream (Milkaut S.A., Santa Fe, Argentina) and condensed sweet milk (Nestle S.A., Buenos Aires, Argentina) were purchased at local markets. The composition of both materials supplied by manufacturers was as follows: (1) cream: 46.0% fat, 2.5% carbohydrate, and 1.6% proteins; (2) condensed milk: 60.0% carbohydrate, 7.5% protein, and 4.0% fat. In addition, microparticulated whey proteins powder (Simplesse Dry100, CPKelco US Inc., Atlanta, GA) was used. The composition supplied by the manufacturer was as follows: 52.9% protein, 4.8% fat, and 2.9% moisture. In this case, a suspension was obtained by dissolving the appropriate amount of powder in distilled water with constant agitation in order to obtain a microparticulated whey protein suspension (MWPS) with 30% total solids content.

Rheological measurements at 20 ± 0.5 °C were carried out in triplicate using a Brookfield rheometer model DV3TLVCP (Brookfield Engineering Laboratories Inc., MA) with cone and plate geometry (CPA-51Z and CPA-52Z). Rotational rheometry was performed in the shear rate range of 0.2−192 s^{-1} depending on the sample, and values of the apparent viscosity as a function of shear rate were determined. Experimental density values at 20

DOI: 10.1021/acs.iecr.6b02107
Ind. Eng. Chem. Res. 2016, 55, 9295−9311

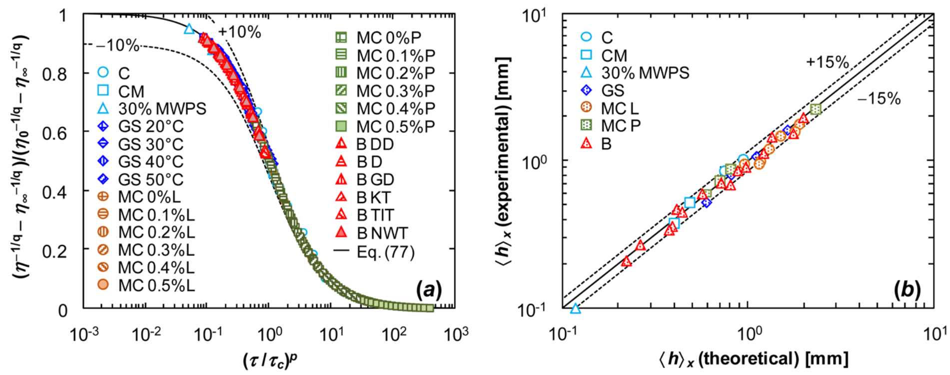

Figure 2. Comparison of experimental and theoretical values of (a) reduced viscosity η^* as a function of $(\tau/\tau_c)^p$ and (b) average film thicknesses $\langle h \rangle_x$ for several suspensions. Suspensions are codified as follows: C: cream, CM: condensed milk, 30% MWPS: microparticulate whey protein suspension with 30% total solids content, GS: glaze suspension, MC x.x%L: milk chocolate with different percentages of lecithin, MC x.x%P: milk chocolate with different percentages of polyglycerol, B DD: batter Dorothy Dawson, B D: batter Drakes, B GD: batter Golden Dipt, B KT: batter Kikkoman tempura, B TIT: batter Tung-I tempura, B NWT: batter Newly Wed tempura. Dashed lines correspond of 10% error in (a) and 15% of error in (b).

°C were determined gravimetrically (5 replicates) by weighing a recipient with known volume (1.83 cm^3) containing an aliquot of each sample.[35] Details of the physical properties of the film-forming fluids are shown in Table 1.

Average film thickness values at 20 °C of cream, condensed milk, and MWPS were obtained by quintuplicate using the dip-coating methodology proposed by Cisneros-Zevallos and Krochta[34] with modifications.[35] Glass plates (L = 40 mm) were used as substrate with different draining times depending on samples (cream: 10 and 30 s, condensed milk: 5, 10, 30, and 60 s, MWPS: 30 s).

2.8.2. Experimental Data from the Literature. Rheological properties, densities, and average film thickness values of several food-grade film-forming fluids obtained from the literature were used (Table 1): a commercial food glaze suspension[35] (substrate: glass plates, L = 40 mm, draining time: 30 s), milk chocolate with different percentages of lecithin and polyglycerol[9] (substrate: acrylic plates, L = 44.5 mm, draining time: 20 s), and six trademarks of adhesion and tempura deep-fat frying commercial batters[10] (substrate: poly methyl methacrylate plates, L = 40 mm, draining times: 60 and 120 s).

2.8.3. Validation Procedure. Fluid physical properties and model parameters fitted to the dimensional form of eq 38 are summarized in Table 1. This data are considered important ready-to-use information useful as quick reference for further analysis in the Results and Discussion section.

The validation process was performed taking into account the adjustment capacity of the viscosity in a wide range of shear stress values and the ability of the mathematical model to predict values of $\langle h \rangle_x$. As a first step, prior to the calculation of the theoretical values of $\langle h \rangle_x$, the parameters of eq 24 were found by minimizing the mean absolute percentage error ($MAPE$) presented in eq 76 using the viscosity data for each suspension:

$$MAPE = \frac{100}{N} \sum_{i=1}^{N} \sqrt{\left[1 - \frac{a_i(\text{theoretical})}{a_i(\text{experimental})}\right]^2} \tag{76}$$

where N is the number of viscosity data points in each suspension presented in Table 1 and a_i are the theoretical and experimental values of η. Then, viscosity data were conveniently rearranged as reduced viscosity η^* using eq 77.

$$\eta^* = \frac{\eta^{-1/q} - \eta_\infty^{-1/q}}{\eta_0^{-1/q} - \eta_\infty^{-1/q}} = \frac{1}{1 + (\tau/\tau_c)^p} \tag{77}$$

The model prediction level of the values of $\langle h \rangle_x$ was calculated using eq 76. In this case, N is the number of suspensions presented in Table 1 and a_i are the theoretical (estimated with eq 84) and experimental values of $\langle h \rangle_x$.

3. RESULTS AND DISCUSSION

3.1. Theoretical Range of Validity of the Approach. As stated in Section 2.2, some assumptions need to be made in order to obtain useful forms of eqs 20−22. First, a natural and conservative way to estimate U is to define (from eq 22) St = $\rho g h_L^2/(\eta_{ref} U) = 1$ and, consequently, $U = \rho g h_L^2/\eta_{ref}$. Second, the minimum (and conservative) value for η_{ref} in a shear-thinning fluid estimated by eq 24 is η_∞. Therefore, $\eta_{ref} = \eta_\infty$. Taking into account eq 20 and replacing the definitions of U and η_{ref} in eq 21, the set of equations that represents the conditions assumed to be true to verify the range of validity of the approach is

$$\frac{h_L}{L} \ll 1 \tag{78}$$

$$\frac{g_x \rho^2 h_L^3}{\eta_\infty^2} \leq 1 \tag{79}$$

3.2. Model Validation. One step of the validation process was the analysis of the viscosity adjustment capacity of the extended Quemada model (dimensional form of eq 38) in a wide range of shear stress. The comparison of the experimental and theoretical values of reduced viscosity η^* as a function of $(\tau/\tau_c)^p$ for the representative concentrated dispersions used as film-forming fluids is shown in Figure 2a. According to the obtained results, values of theoretical η^* obtained by using eq 77 fitted satisfactorily to all experimental viscosity data in a considerable range of shear stress values, obtaining $MAPE$ errors lower than 8% (Table 1). The level of data description obtained by using the conveniently rearranged eq 77 indicates a good capability to be used as a viscosity model for describing the behavior of several complex concentrated dispersions in a wide range of viscosities (0.01−228 Pa s), shear stresses (0.1−463 Pa), temperatures (20−50 °C), and ingredient concentrations or total solids contents (Table 1). Moreover, the complex nature of each film-forming fluid used in this work must be taken into account to

DOI: 10.1021/acs.iecr.6b02107
Ind. Eng. Chem. Res. 2016, 55, 9295−9311

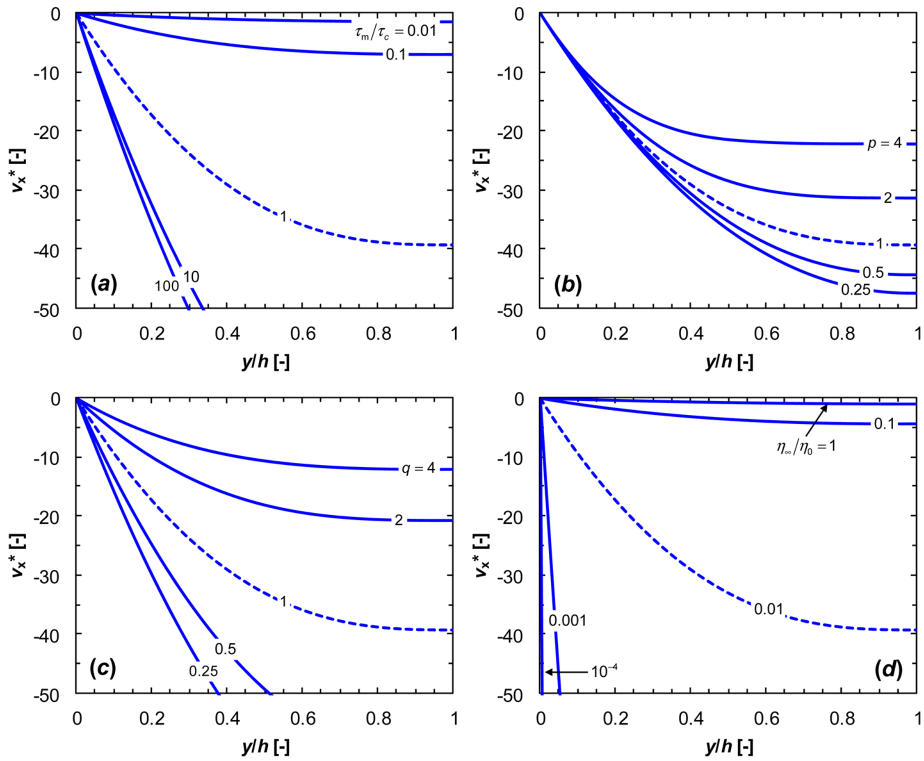

Figure 3. Dimensionless velocity v_x^* as a function of the nondimensional position y/h for different values of (a) τ_m/τ_c, (b) p, (c) q, and (d) η_∞/η_0. The condition adopted as reference is represented by a dashed line and has the values of $\tau_m/\tau_c = p = q = 1$ and $\eta_\infty/\eta_0 = 0.01$.

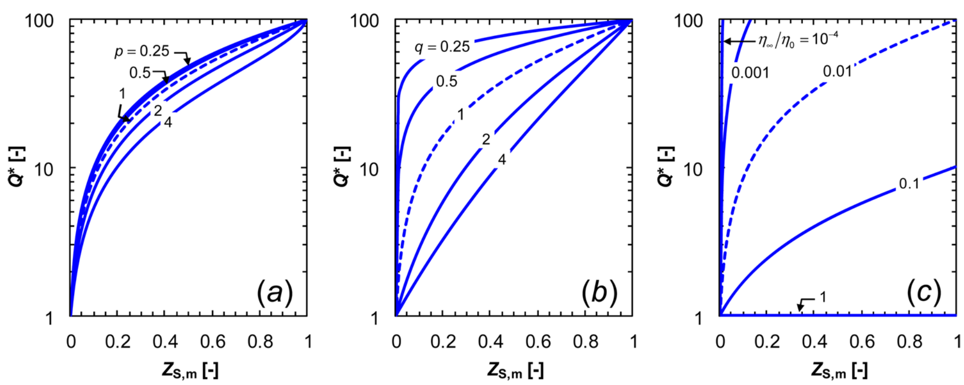

Figure 4. Reduced flow rate Q^* as a function of the normalized and dimensionless shear stress parameter $Z_{S,m}$ for different values of (a) p, (b) q, and (c) η_∞/η_0. The condition adopted as reference is represented by a dashed line and has the values of $p = q = 1$ and $\eta_\infty/\eta_0 = 0.01$.

emphasize the adjustment capacity of the extended Quemada model. For example, cream can be considered a concentrated emulsion, where milk fat globules are dispersed in the aqueous phase. Condensed milk is a complex dispersion (emulsion/suspension), where colloidal particles (caseins), solid sugar particles, and milk fat globules are dispersed in a continuous aqueous phase. In the microparticulated whey protein and glaze suspensions, a high concentration of solid particles (30% and 83.33% of total solids content, respectively) is dispersed in the aqueous phase.[35] Milk chocolate can be considered a complex suspension, where solid particles (cocoa, sugar, and milk) are dispersed in a continuous lipid phase (cocoa butter, milk fat, and emulsifier).[9] Adhesion and tempura deep-fat frying batters are highly complex dispersion (aerated suspension), because solid particles (50% total solids content, mainly wheat flour) are dispersed in a continuous aqueous phase with mixing (270−300 rpm during 3−4 min).[10]

The other step of the validation process was the study of the mathematical model ability to predict values of $\langle h \rangle_x$. The comparison between experimental and theoretical average film thickness values for the representative concentrated dispersions used in this work is shown in Figure 2b. Theoretical values of $\langle h \rangle_x$ were estimated by using eq 84 and physical properties and rheological parameters of the film-forming fluids presented in Table 1. The range of experimental $\langle h \rangle_x$ values used for each dispersion was as follows: cream, 0.89−1.06 mm; condensed milk, 0.38−1.01 mm; MWPS, 0.14 mm; glaze suspension, 0.53−1.52 mm; milk chocolate with different percentages of lecithin and polyglycerol, 0.60−4.60 mm; deep-fat frying batters, 0.20−2.00 mm (Figure 2b). According to the obtained results, a satisfactory agreement was observed between experimental and theoretical average film thickness values, with the prediction errors lower than 15%. It is interesting to notice that the mathematical model developed in this work can predict a wide

DOI: 10.1021/acs.iecr.6b02107
Ind. Eng. Chem. Res. 2016, 55, 9295−9311

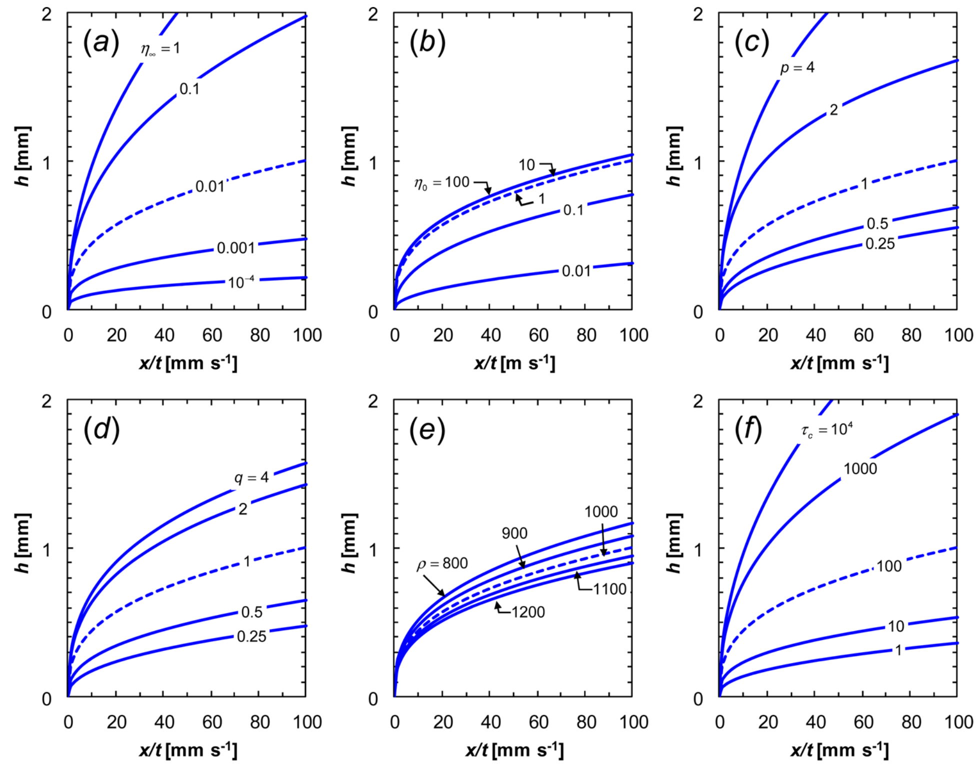

Figure 5. Film thickness h as a function of the nondimensional space−time variable x/t for different values of (a) η_∞, (b) η_0, (c) p, (d) q, (e) ρ, and (f) τ_c. The condition adopted as reference is represented by a dashed line and has the values of $\eta_\infty = 0.01$ Pa s, $\eta_0 = 1$ Pa s, $p = 1$, $q = 1$, $\rho = 1000$ kg m^{-3}, and $\tau_c = 100$ Pa.

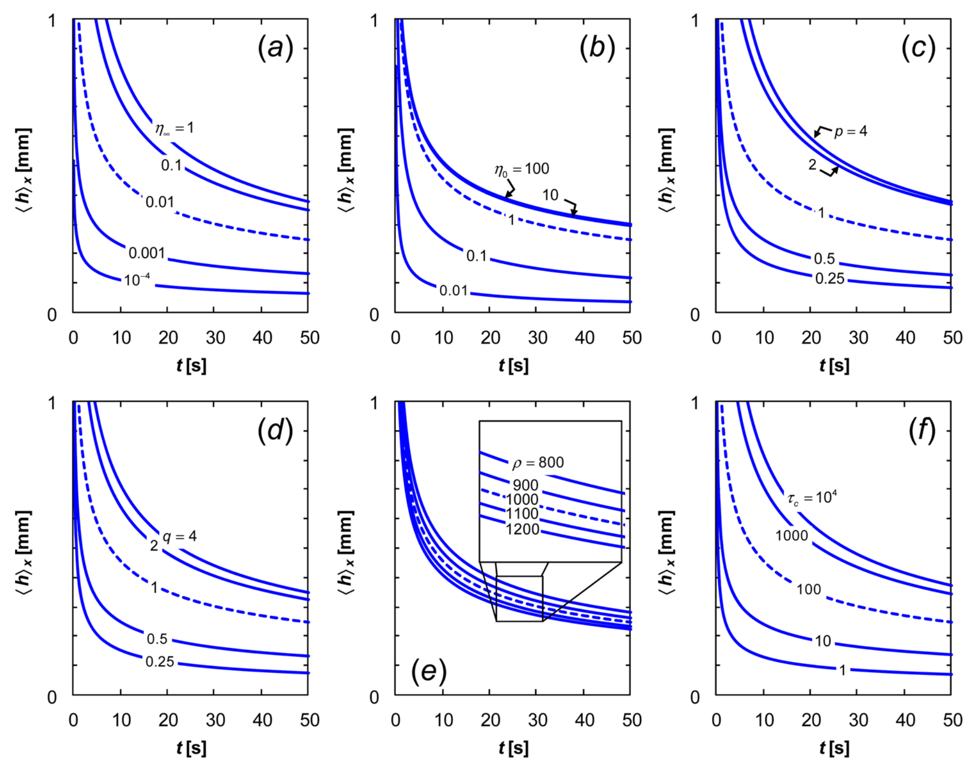

Figure 6. Average film thickness $\langle h \rangle_x$ as a function of time t for different values of (a) η_∞, (b) η_0, (c) p, (d) q, (e) ρ, and (f) τ_c. The condition adopted as reference is represented by a dashed line and has the values of $\eta_\infty = 0.01$ Pa s, $\eta_0 = 1$ Pa s, $p = 1$, $q = 1$, $\rho = 1000$ kg m^{-3}, and $\tau_c = 100$ Pa.

range of average film thicknesses (0.14−4.6 mm) that can be obtained during a dip-coating draining stage (with several substrates, plate lengths, and draining times) using concentrated dispersions.

DOI: 10.1021/acs.iecr.6b02107
Ind. Eng. Chem. Res. 2016, 55, 9295−9311

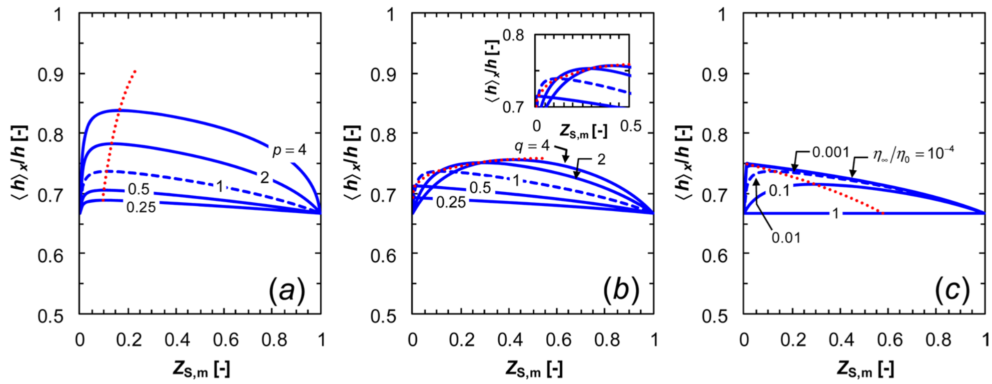

Figure 7. Ratio of the average film thickness to the local film thickness $\langle h \rangle_x/h$ as a function of the normalized and dimensionless shear stress parameter $Z_{S,m}$ for different values of (a) p, (b) q, and (c) η_∞/η_0. Red dotted line represents maximum points in profiles. The condition adopted as reference is represented by a dashed line and has the values of $p = q = 1$ and $\eta_\infty/\eta_0 = 0.01$.

3.3. Model Sensitivity Analysis. A sensitivity analysis was performed to assess the effect of varying parameters in the mathematical model on the main predicted variables. It is important to mention that this analysis is only partial and further studies need to be made to show the full capabilities of eq 24. For economy reasons, only the expressions resulting from using eq 38 (*i.e.* $\eta = \eta(\tau)$) were presented and studied in the analysis. However, *a priori*, the results can be used to estimate qualitatively the behavior of the model when $\eta = \eta(\dot{\gamma})$. Also, Figures 3–Figure 7 were presented using a reference condition to help in the analysis. This reference (dashed lines) corresponds to a fluid with a similar behavior shown by an aqueous suspension of locus beam gum and sucrose[36,37] (described by η_∞ = 0.01 Pa s, η_0 = 1 Pa s, p = 1, q = 1, ρ = 1000 kg m^{-3}, and τ_c = 100 Pa).

3.3.1. Velocity Profile. Figure 3 shows the normalized velocity (v_x^*) as a function of the dimensionless position (y/h) for several expected values of τ_m/τ_c, p, q, and η_∞/η_0. These profiles were obtained by using eq 38 to estimate η. For all cases, the velocity values exhibit smooth profiles where the minimum and maximum values are located at $y/h = 0$ (surface of the substrate) and $y/h = 1$ (interface film–air), respectively. First, an increment in τ_m/τ_c produces an increment in v_x^* (Figure 3a). This behavior is observed regardless of whether τ_m/τ_c is greater or less than 1. The effect of τ_m/τ_c on the velocity profiles is less pronounced as it moves away from 1 due to the asymptotic behavior of η as $\tau_m/\tau_c \to 0$ (*i.e.* $\eta \to \eta_0$) or $\tau_m/\tau_c \to \infty$ (*i.e.* $\eta \to \eta_\infty$). Second, Figure 3b shows that an increment in p produces a decrease in v_x^*. This is due to the effect that p has on η (eq 38). An increment in p produces a decrease in η and consequently an increase in v_x^*. The results show that the effect of p on v_x^* decreases as $y/h \to 0$. This is because of the values of τ_m/τ_c, q, and η_∞/η_0, chosen for the comparison. The slope of $v_x^*|_{y=0}$ is $-2\{[1 + (\eta_\infty/\eta_0)^{-1/q}(\tau_m/\tau_c)^p]/[1 + (\tau_m/\tau_c)^p]\}^q$, and for $\tau_m/\tau_c = q = 1$ and $\eta_\infty/\eta_0 = 0.01$, $[\partial v_x^*/\partial(y/h)]_{y=0} = -101$ (i.e., constant). Third, similarly as in the case of p, an increment in q produces a decrease in v_x^* (Figure 3*c*). This time, there is no evidence of constancy for the slope of v_x^* as $y/h \to 0$. Fourth, an increment in η_∞/η_0 (within the expected range for a shear-thinning type of fluid) produces a marked decrease in v_x^*. Figure 3, which shows that the parameter that most affected v_x^* is η_∞/η_0, followed by τ_m/τ_c, q, and finally p.

3.3.2. Flow Rate. The dimensionless flow rate Q^* profiles as a function of the normalized and dimensionless shear stress parameter $Z_{S,m}$ for selected values of p, q, and η_∞/η_0 are shown in Figure 4. In general, an increase in $Z_{S,m}$ produces an increase in the flow rate. This behavior can be explained by analyzing eq 46. Higher values of $Z_{S,m}$ represent higher values of h or ρ (i.e., more mass flowing) and lower values of τ_c (i.e., a higher fraction of the shear stress is higher than τ_c, which results in $\eta \to \eta_\infty$ for shear-thinning type of fluids). Also, profiles show concavity for the selected values of p, q, and η_∞/η_0. That is, high increments in Q^* were obtained for low values and increments in $Z_{S,m}$. Figure 4a shows that an increment in p results in a decrease in the values of Q^* (higher values of p produce more viscous films). Similar results on Q^* were observed for selected values of q (Figure 4b). In general, as q increased, higher values of η were produced. In the case of the third parameter (Figure 4c), an increase in η_∞/η_0 (selected values lower or equal to 1) produced a decrease in Q^*. The maximum value of Q^* obtained at $Z_{S,m} = 1$ is an inverse function of η_∞/η_0. Then, for example using η_∞/η_0 = 0.01, $Q^*|_{Z_{S,m}=1} = 100$ is obtained. Finally, comparing the effect of the parameters, the one that most affected Q^* was η_∞/η_0, followed by q, and finally p.

3.3.3. Local Film Thickness. Local film thickness h profiles as a function of the space–time x/t variable for selected values of η_∞, η_0, p, q, ρ ,and τ_c are shown in Figure 5. These profiles were obtained using a dimensional form of eq 69. In general, an increment in x or a decrement in t causes a parabolic-like increment in h. In the case of η_∞, an increment in this parameter produces an increase in the local film thickness. This is due to the increased resistance of the film to drain from the substrate. A similar behavior is observed for an increment in η_0. In this case, an asymptotic profile is observed for $\eta_0 > 10$. This performance can be explained by observing the asymptotic nature of η for a given value of h. Particularly for the set of values adopted for η_∞, η_0, p, q, ρ, and τ_c, values of η_0 higher than 10 produce negligible changes in η. Figure 5 shows that an increment in p (Figure 5c) and q (Figure 5d) produces an increment in h. This is because higher values of those parameters (within the range of the selected values) result in higher viscosity values (higher resistance to drain) and consequently more film on the substrate at any time. In the rest of the variables, a decrease in density of the film (Figure 5e) and an increase in τ_c (Figure 5f) resulted in thicker films. On one hand, higher density values result in higher gravitational forces acting on the film to produce draining. On the other hand, higher values of τ_c, for a given film thickness, result in higher viscosities and consequently lower draining velocities. The parameters that most affected h were η_∞, p, and τ_c.

3.3.4. Average Film Thickness. Profiles of the average film thickness as a function of time for selected values of η_∞, η_0, p, q, ρ, and τ_c are shown in Figure 6. In this figure, profiles were obtained

DOI: 10.1021/acs.iecr.6b02107
Ind. Eng. Chem. Res. 2016, 55, 9295–9311

at $x = 40$ mm. In general, a convex functionality of the type $\langle h\rangle_x \sim at^{-b}$ (where a, $b > 0$) is observed. Similar functionality was obtained by Peralta et al.[15] It is important to note that as $t \to 0$ the $\langle h\rangle_x \to \infty$. This is because of the initial conditions imposed for this example. The effect of η_∞, η_0, p, q, ρ, and τ_c produced on $\langle h\rangle_x$ was similar to the one observed for h (Figure 5). Briefly, an increase in η_∞, η_0, p, q, and τ_c and a decrease in ρ produced an increase in $\langle h\rangle_x$. Also, the magnitude of the effect of the parameters on $\langle h\rangle_x$ is conserved compared to the one observed for h. It is important to keep in mind that these effects may not be observed for another combination of the parameter values.

3.3.5. Film Thickness Homogeneity. Figure 7 shows the ratio of the average film thickness to the local film thickness $\langle h\rangle_x/h$ profiles as a function of the normalized and dimensionless shear stress parameter $Z_{S,m}$ for selected values of p, q, and η_∞/η_0. It is important to mention that $\langle h\rangle_x/h$ can be regarded as a degree of thickness homogeneity of the film.[14] A high value in thickness homogeneity can be a desirable attribute in a given film depending on the characteristics of the final product. Therefore, the quantification of this parameter could be very important to characterize a coating material or a process.

In general, $\langle h\rangle_x/h$ profiles show a concave functionality with respect to $Z_{S,m}$. All profiles presented a maximum and a value of $\langle h\rangle_x/h = {}^2/_3$ at the extremes (*i.e.* $Z_{S,m} = 0$ and $Z_{S,m} = 1$). Values of ${}^2/_3$ in $\langle h\rangle_x/h$ are obtained for shear-independent viscosity materials (for example: Newtonian materials).[14,15] This is explained due to the fact that as $|\underline{\underline{\tau}}| \to 0$ (*i.e.* $Z_{S,m} = 0$) and $|\underline{\underline{\tau}}| \to \infty$ (*i.e.* $Z_{S,m} = 1$), the viscosity approaches the constant values of η_0 and η_∞, respectively.

In all cases, an increment in p and q, and a reduction in η_∞/η_0, produced higher values of $\langle h\rangle_x/h$ (i.e., more homogeneous films) for $0 < Z_{S,m} < 1$.

As mentioned before, a material described by eq 38 produces a maximum in $\langle h\rangle_x/h$ as a function of $Z_{S,m}$. These extrema (red dotted lines in Figure 7) can be found by differentiating eq 73 with respect to $Z_{S,m}$ and equating to zero the resulting expression. This procedure yields

$$3 - \frac{(1 - Z_{S,me})^{3/p}\{3 - [3 + qp(1 - Z_{S,me})]\eta_c Z_{S,me}\}}{(1 - \eta_c Z_{S,me})^{1+q}} \times F_1\left(\frac{3}{p}; \frac{3}{p} + 1, -q; \frac{3}{p} + 1; Z_{S,me}, \eta_c Z_{S,me}\right) = 0 \quad (80)$$

where $Z_{S,me}$ is the normalized and dimensionless shear stress parameter that produces a maximum value in $\langle h\rangle_x/h$.

Specifically, in the case of p, the maxima (red dotted line) were obtained at $0.1 < Z_{S,m} < 0.3$ for $0.25 < p < 10$. The maximum values of $\langle h\rangle_x/h$ increased as p increased. Similar results were obtained for q. In this case maximum values of $\langle h\rangle_x/h$ were obtained in a broader range: $0 < Z_{S,m} < 0.5$. These maximum values were in the range of $0.666 < (\langle h\rangle_x/h)_{max} < 0.758$. Conversely, the extrema of $\langle h\rangle_x/h$ decreased as η_∞/η_0 increased (red dotted line in Figure 7c). In this case, the maximum value of the extrema is 0.75, which is obtained at $Z_{S,m} \to 0$ when $\eta_\infty/\eta_0 \to 0$.

3.4. Dimensional Forms of the Main Variables and Special Cases. Similarly to the model presented by Peralta et al.,[14] the expressions obtained in this work were simplified using the well-known and important special cases of the generalized Quemada model (eq 24) mentioned in Section 2.3. These expressions are novel analytical solutions resulting from a thorough simplification procedure using mathematical identities from Peralta et al.[14] and Weisstein.[38] Also, it is important to mention that their presentation would usually require separate studies.

3.4.1. Generalized Quemada.

- When $\eta = \eta(\tau)$:

$$\eta = \eta_\infty[1 + (\tau/\tau_c)^p]^q/[(\eta_\infty/\eta_0)^{1/q} + (\tau/\tau_c)^p]^q$$

$$v_x = \frac{\tau_c^2}{2\rho g_x \eta_0} \times \left\{\begin{aligned} &Z_{S,m}^{2/p} F_1\left(\frac{2}{p}; \frac{2}{p} + 1, -q; \frac{2}{p} + 1; Z_{S,m}, \eta_c Z_{S,m}\right) \\ &- Z_S^{2/p} F_1\left(\frac{2}{p}; \frac{2}{p} + 1, -q; \frac{2}{p} + 1; Z_S, \eta_c Z_S\right)\end{aligned}\right\} \quad (81)$$

$$Q = \frac{\tau_m^3}{3(\rho g_x)^2 \eta_0}(1 - Z_{S,m})^{3/p} \times F_1\left(\frac{3}{p}; \frac{3}{p} + 1, -q; \frac{3}{p} + 1; Z_{S,m}, \eta_c Z_{S,m}\right) \quad (82)$$

$$\left[\frac{(\rho g_x)^{qp+1}}{\eta_\infty \tau_c^{qp}(x/t)}\right]^{1/q} h^{p+2/q} + \left[\frac{\rho g_x}{\eta_0(x/t)}\right]^{1/q} h^{2/q} - \left(\frac{\rho g_x}{\tau_c}\right)^p h^p - 1 = 0 \quad (83)$$

$$\frac{\langle h\rangle_x}{h} = 1 - \frac{1}{3}\frac{(1 - Z_{S,m})^{3/p}}{(1 - \eta_c Z_{S,m})^q} \times F_1\left(\frac{3}{p}; \frac{3}{p} + 1, -q; \frac{3}{p} + 1; Z_{S,m}, \eta_c Z_{S,m}\right) \quad (84)$$

- When $\eta = \eta(\dot\gamma)$:

$$\eta = \eta_\infty[1 + (\dot\gamma/\dot\gamma_c)^p]^q/[(\eta_\infty/\eta_0)^{1/q} + (\dot\gamma/\dot\gamma_c)^p]^q$$

$$v_x = \frac{\eta_0 \dot\gamma_c^2}{2\rho g_x}\left\{\begin{aligned} &Z_{R,m}^{2/p} F_1\left(\frac{2}{p}; \frac{2}{p} + 1, q; \frac{2}{p} + 1; Z_{R,m}, \eta_c Z_{R,m}\right) \\ &+ \frac{2q\eta_c p}{(2 + p)} Z_{R,m}^{2/p+1} F_1\left(\frac{2}{p} + 1; \frac{2}{p}, 1 + q; \frac{2}{p} + 2; Z_{R,m}, \eta_c Z_{R,m}\right) \\ &- Z_R^{2/p} F_1\left(\frac{2}{p}; \frac{2}{p} + 1, q; \frac{2}{p} + 1; Z_R, \eta_c Z_R\right) \\ &- \frac{2q\eta_c p}{(2 + p)} Z_R^{2/p+1} F_1\left(\frac{2}{p} + 1; \frac{2}{p}, 1 + q; \frac{2}{p} + 2; Z_R, \eta_c Z_R\right)\end{aligned}\right\} \quad (85)$$

DOI: 10.1021/acs.iecr.6b02107
Ind. Eng. Chem. Res. 2016, 55, 9295−9311

$$Q = \frac{\dot{\gamma}_m^3 \eta_0^2}{(\rho g_x)^2}\left\{\frac{q\eta_c p}{(3+p)} Z_{\mathrm{R,m}}(1-Z_{\mathrm{R,m}})^{3/p} \times F_1\left(\frac{3}{p}+1;\ \frac{3}{p},\ 1+2q;\ \frac{3}{p}+2;\ Z_{\mathrm{R,m}},\ \eta_c Z_{\mathrm{R,m}}\right) + \frac{2}{p^2}(1-Z_{\mathrm{R,m}})^{3/p} F_1\left(\frac{3}{p};\ \frac{3}{p}+1,\ 2q;\ \frac{3}{p}+1;\ Z_{\mathrm{R,m}},\ \eta_c Z_{\mathrm{R,m}}\right)\right\} \quad (86)$$

$$\left[\frac{\rho g_x \dot{\gamma}_c^{qp}}{\eta_0 (x/t)^{qp+1}}\right]^{1/q} h^{p+2/q} + \left[\frac{\rho g_x}{\eta_\infty (x/t)}\right]^{1/q} h^{2/q} - \left[\frac{\dot{\gamma}_c}{(x/t)}\right]^p h^p - 1 = 0 \quad (87)$$

$$\frac{\langle h\rangle_x}{h} = 1 - (1-Z_{\mathrm{R,m}})^{3/q}(1-\eta_c Z_{\mathrm{R,m}})^{2q} \times \left[\frac{q\eta_c p}{(3+p)} Z_{\mathrm{R,m}} F_1\left(\frac{3}{p}+1;\ \frac{3}{p},\ 2q+1;\ \frac{3}{p}+2;\ Z_{\mathrm{R,m}},\ \eta_c Z_{\mathrm{R,m}}\right) + \frac{1}{3} F_1\left(\frac{3}{p};\ \frac{3}{p}+1,\ 2q;\ \frac{3}{p}+1;\ Z_{\mathrm{R,m}},\ \eta_c Z_{\mathrm{R,m}}\right)\right] \quad (88)$$

3.4.2. Quemada.

- When $\eta = \eta(\tau)$:

$$\eta = \eta_\infty[1 + (\tau/\tau_c)^p]^2/[(\eta_\infty/\eta_0)^{1/2} + (\tau/\tau_c)^p]^2$$

$$v_x = \frac{\tau_c^2}{2\rho g_x \eta_0} \times \left\{\frac{Z_{\mathrm{S,m}}^{2/p}}{(1-Z_{\mathrm{S,m}})^{2/p}}\left\{1 - \frac{2\eta_c^2}{p} Z_{\mathrm{S,m}} + 2\eta_c \left[\frac{\eta_c}{p} - \frac{2p}{(2+p)}\right] Z_{\mathrm{S,m}\,2}F_1\left(1,\ 1;\ \frac{2}{p}+2;\ Z_{\mathrm{S,m}}\right)\right\} - \frac{Z_{\mathrm{S}}^{2/p}}{(1-Z_{\mathrm{S}})^{2/p}}\left\{1 - \frac{2\eta_c^2}{p} Z_{\mathrm{S}} + 2\eta_c\left[\frac{\eta_c}{p} - \frac{2p}{(2+p)}\right] Z_{\mathrm{S}\,2}F_1\left(1,\ 1;\ \frac{2}{p}+2;\ Z_{\mathrm{S}}\right)\right\}\right\} \quad (89)$$

$$Q = \frac{\tau_{\mathrm{m}}^3}{(\rho g_x)^2 \eta_0}\left[\frac{1}{3} - \frac{\eta_c^2}{p} Z_{\mathrm{S,m}} + \eta_c \frac{[\eta_c(3+p) - 2p]}{d(3+p)} Z_{\mathrm{S,m}} \times {}_2F_1\left(1,\ 1;\ \frac{3}{p}+2;\ Z_{\mathrm{S,m}}\right)\right] \quad (90)$$

$$h^p - \left(\frac{\eta_\infty}{\rho g_x}\frac{x}{t}\right)^{1/2} h^{p-1} + \left(\frac{\tau_c}{\rho g_x}\right)^p \left(\frac{\eta_\infty}{\eta_0}\right)^{1/2} - \left(\frac{\tau_c}{\rho g_x}\right)^p \left(\frac{\eta_\infty}{\rho g_x}\frac{x}{t}\right)^{1/2} h^{-1} = 0 \quad (91)$$

$$\frac{\langle h\rangle_x}{h} = 1 - \frac{1}{3}\frac{(1-Z_{\mathrm{S,m}})^{3/p}}{(1-\eta_c Z_{\mathrm{S,m}})^2} F_1\left(\frac{3}{p};\ \frac{3}{p}+1,\ -2;\ \frac{3}{p}+1;\ Z_{\mathrm{S,m}},\ \eta_c Z_{\mathrm{S,m}}\right) \quad (92)$$

where ${}_2F_1[a,b;c;s]$ is the Gauss hypergeometric function.[32]

- When $\eta = \eta(\dot{\gamma})$:

$$\eta = \eta_\infty[1 + (\dot{\gamma}/\dot{\gamma}_c)^p]^2/[(\eta_\infty/\eta_0)^{1/2} + (\dot{\gamma}/\dot{\gamma}_c)^p]^2$$

$$v_x = \frac{\eta_0 \dot{\gamma}_c^2}{2\rho g_x}\left[Z_{\mathrm{R,m}}^{2/p} F_1\left(\frac{2}{p};\ \frac{2}{p}+1,\ 2;\ \frac{2}{p}+1;\ Z_{\mathrm{R,m}},\ \eta_c Z_{\mathrm{R,m}}\right) + \frac{4\eta_c p}{(2+p)} Z_{\mathrm{R,m}}^{2/p+1} \times F_1\left(\frac{2}{p}+1;\ \frac{2}{p},\ 3;\ \frac{2}{p}+2;\ Z_{\mathrm{R,m}},\ \eta_c Z_{\mathrm{R,m}}\right) - Z_{\mathrm{R}}^{2/p} F_1\left(\frac{2}{p};\ \frac{2}{p}+1,\ 2;\ \frac{2}{p}+1;\ Z_{\mathrm{R}},\ \eta_c Z_{\mathrm{R}}\right) - \frac{4\eta_c p}{(2+p)} Z_{\mathrm{R}}^{2/p+1} \times F_1\left(\frac{2}{p}+1;\ \frac{2}{p},\ 3;\ \frac{2}{p}+2;\ Z_{\mathrm{R}},\ \eta_c Z_{\mathrm{R}}\right)\right] \quad (93)$$

$$Q = \frac{\dot{\gamma}_{\mathrm{m}}^3 \eta_0^2}{(\rho g_x)^2} \times \left\{\frac{2\eta_c p}{(3+p)} Z_{\mathrm{R,m}}(1-Z_{\mathrm{R,m}})^{3/p} \times F_1\left(\frac{3}{p}+1;\ \frac{3}{p},\ 5;\ \frac{3}{p}+2;\ Z_{\mathrm{R,m}},\ \eta_c Z_{\mathrm{R,m}}\right) + \frac{1}{3}(1-Z_{\mathrm{R,m}})^{3/p} \times F_1\left(\frac{3}{p};\ \frac{3}{p}+1,\ 4;\ \frac{3}{p}+1;\ Z_{\mathrm{R,m}},\ \eta_c Z_{\mathrm{R,m}}\right)\right\} \quad (94)$$

$$h^{p+1} - \left(\frac{\eta_0}{\rho g_x}\frac{x}{t}\right)^{1/2} h^p + \frac{1}{\dot{\gamma}_c^p}\left(\frac{\eta_0}{\eta_\infty}\right)^{1/2}\left(\frac{x}{t}\right)^p h - \frac{1}{\dot{\gamma}_c^p}\left(\frac{\eta_0}{\rho g_x}\frac{x}{t}\right)^{1/2}\left(\frac{x}{t}\right)^p = 0 \quad (95)$$

$$\frac{\langle h\rangle_x}{h} = 1 - (1-Z_{\mathrm{R,m}})^{3/p}(1-\eta_c Z_{\mathrm{R,m}})^4 \left\{\frac{2\eta_c p}{(3+p)} Z_{\mathrm{R,m}} F_1\left(\frac{3}{p}+1;\ \frac{3}{p},\ 5;\ \frac{3}{p}+2;\ Z_{\mathrm{R,m}},\ \eta_c Z_{\mathrm{R,m}}\right) + \frac{1}{3} F_1\left(\frac{3}{p};\ \frac{3}{p}+1,\ 4;\ \frac{3}{p}+1;\ Z_{\mathrm{R,m}},\ \eta_c Z_{\mathrm{R,m}}\right)\right\} \quad (96)$$

DOI: 10.1021/acs.iecr.6b02107
Ind. Eng. Chem. Res. 2016, 55, 9295−9311

3.4.3. Berli–Quemada — $\eta = \eta_\infty[1 + (\tau/\tau_c)^2]/[(\eta_\infty/\eta_0)^{1/2} + (\tau/\tau_c)]^2$.

$$v_x = \frac{\tau_c^2}{2\rho g_x \eta_0}\left\{\frac{Z_{S,m}^2}{(1-Z_{S,m})^2} - \frac{2\eta_c^2 Z_{S,m}^3}{(1-Z_{S,m})^2} + \eta_c(3\eta_c - 2)\frac{Z_{S,m}(3Z_{S,m}-2)}{(1-Z_{S,m})^2} - 2\eta_c(3\eta_c-2)\ln(1-Z_{S,m}) - \frac{Z_S^2}{(1-Z_S)^2} + \frac{2\eta_c^2 Z_S^3}{(1-Z_S)^2} - \eta_c(3\eta_c-2)\frac{Z_S(3Z_S-2)}{(1-Z_S)^2} + 2\eta_c(3\eta_c-2)\ln(1-Z_S)\right\} \quad (97)$$

$$Q = \frac{\tau_m^3}{3(\rho g_x)^2\eta_0}[1 - 11\eta_c + 22\eta_c^2 + 6\eta_c(2\eta_c-1)Z_{S,m}^{-2} - 15\eta_c(2\eta_c-1)Z_{S,m}^{-1} - 3\eta_c^2 Z_{S,m} + 6\eta_c(2\eta_c-1)Z_{S,m}^{-3}(1-Z_{S,m})^3\ln(1-Z_{S,m})] \quad (98)$$

$$h = -\frac{1}{2}\left[\left(\frac{\tau_c}{\rho g_x}\right)\left(\frac{\eta_\infty}{\eta_0}\right)^{1/2} - \left(\frac{\eta_\infty}{\rho g_x}\frac{x}{t}\right)^{1/2}\right] + \frac{1}{2}\sqrt{\left[\left(\frac{\tau_c}{\rho g_x}\right)\left(\frac{\eta_\infty}{\eta_0}\right)^{1/2} - \left(\frac{\eta_\infty}{\rho g_x}\frac{x}{t}\right)^{1/2}\right]^2 + 4\left(\frac{\tau_c}{\rho g_x}\right)\left(\frac{\eta_\infty}{\rho g_x}\frac{x}{t}\right)^{1/2}} \quad (99)$$

$$\frac{\langle h\rangle_x}{h} = \left\{Z_{S,m}\{\{-4Z_{S,m}^2 + \eta_c\{-6 + Z_{S,m}[15 + (6Z_{S,m} - 11)]\}\} + 6\eta_c(1-Z_{S,m})^3\ln(1-Z_{S,m})\}\right\} \Big/ \left[6Z_{S,m}^3(-1 + \eta_c Z_{S,m})\right] \quad (100)$$

3.4.4. Heinz–Casson — $\eta = \eta_\infty[1 + (\dot\gamma/\dot\gamma_c)^p]^{1/p}/[(\eta_\infty/\eta_0)^p + (\dot\gamma/\dot\gamma_c)^p]^{1/p}$.

$$v_x = \frac{\dot\gamma_c^2\eta_\infty}{\rho g_x(1+p)}\left[\frac{Z_{R,m}^{1/p+1}}{(1-Z_{R,m})^{2/p}} \times {}_2F_1\left(1, 1-\frac{1}{p}; 2+\frac{1}{p}; Z_{R,m}\right) - \frac{Z_R^{1/p+1}}{(1-Z_R)^{2/p}} \times {}_2F_1\left(1, 1-\frac{1}{p}; 2+\frac{1}{p}; Z_R\right)\right] \quad (101)$$

$$Q = \frac{\gamma_m^3\eta_\infty^2}{(\rho g_x)^2(1+p)} Z_{R,m}^{1-2/p}\,{}_2F_1\left(1, 1-\frac{2}{p}; 2+\frac{1}{p}; Z_{R,m}\right) \quad (102)$$

$$h^{2p} - \left(\frac{\eta_\infty\dot\gamma_c}{\rho g_x}\right)^p h^p - \left(\frac{\eta_\infty}{\rho g_x}\frac{x}{t}\right)^p = 0 \quad (103)$$

$$\frac{\langle h\rangle_x}{h} = 1 - \frac{Z_{R,m}}{(1+p)}{}_2F_1\left(1, 1-\frac{2}{p}; \frac{1}{p}+2; Z_{R,m}\right) \quad (104)$$

3.4.5. Casson — $\eta = \eta_\infty[1 + (\dot\gamma/\dot\gamma_c)^{1/2}]^2/[(\eta_\infty/\eta_0)^{1/2} + (\dot\gamma/\dot\gamma_c)^{1/2}]^2$.

$$v_x = \frac{\dot\gamma_c^2\eta_\infty}{6\rho g_x}\left[Z_{R,m}^3\frac{(4-Z_{R,m})}{(1-Z_{R,m})^4} - Z_R^3\frac{(4-Z_R)}{(1-Z_R)^4}\right] \quad (105)$$

$$Q = \frac{\dot\gamma_m^3\eta_\infty^2}{30(\rho g_x)^2}\frac{(-Z_{R,m}^3 + 6Z_{R,m}^2 - 15Z_{R,m} + 20)}{Z_{R,m}^3} \quad (106)$$

$$h - \left(\frac{\eta_\infty\dot\gamma_c}{\rho g_x}\right)^{1/2} h^{1/2} - \left(\frac{\eta_\infty}{\rho g_x}\frac{x}{t}\right)^{1/2} = 0 \quad (107)$$

$$\frac{\langle h\rangle_x}{h} = 1 - \frac{1}{30}(20Z_{R,m} - 15Z_{R,m}^2 + 6Z_{R,m}^3 - Z_{R,m}^4) \quad (108)$$

3.4.6. Sisko — $\eta = \eta_\infty + (\eta_\infty/\dot\gamma_c^p)\dot\gamma^p$.

$$v_x = \frac{\eta_\infty\dot\gamma_c^2}{\rho g_x(2+p)}\left\{\frac{(1-Z_{R,m})^{2/p}}{Z_{R,m}^{2/p}}\left[\frac{(1+p)}{Z_{R,m}} - \frac{p}{2}\right] - \frac{(1-Z_R)^{2/p}}{Z_R^{2/p}}\left[\frac{(1+p)}{Z_R} - \frac{p}{2}\right]\right\} \quad (109)$$

$$Q = \frac{\dot\gamma_m^3\eta_\infty^2}{(\rho g_x)^2}\left[\frac{(1+p)}{(3+2p)}\frac{(1-Z_{R,m})^2}{Z_{R,m}^2} + \frac{(2+p)}{(3+p)}\frac{(1-Z_{R,m})}{Z_{R,m}} + \frac{1}{3}\right] \quad (110)$$

$$h^{p+2} - \frac{\eta_\infty}{\rho g_x}\frac{x}{t}h^p - \frac{\eta_\infty}{\rho g_x\dot\gamma_c^p}\left(\frac{x}{t}\right)^{p+1} = 0 \quad (111)$$

$$\frac{\langle h\rangle_x}{h} = \frac{18 + 3p(5 + Z_{R,m}) + p^2(3 + Z_{R,m}^2)}{3(3+2p)(3+p)} \quad (112)$$

3.4.7. Bingham — $\eta = \eta_\infty + \eta_\infty\dot\gamma_c/\dot\gamma$.

$$v_x = \frac{\eta_\infty\dot\gamma_c^2}{2\rho g_x}\left[\frac{Z_{R,m}^2}{(1-Z_{R,m})^2} - \frac{Z_R^2}{(1-Z_R)^2}\right] \quad (113)$$

$$Q = \frac{\dot\gamma_m^3\eta_\infty^2}{6(\rho g_x)^2}\frac{(3-Z_{R,m})}{Z_{R,m}} \quad (114)$$

$$h^2 - \frac{\eta_\infty\dot\gamma_c}{St}h - \frac{\eta_\infty}{St}\frac{x}{t} = 0 \quad (115)$$

$$\frac{\langle h\rangle_x}{h} = \frac{1}{6}Z_{R,m}^2 - \frac{1}{2}Z_{R,m} + 1 \quad (116)$$

3.4.8. Cross — $\eta = \eta_\infty + (\eta_0 - \eta_\infty)/[1 + (\dot\gamma/\dot\gamma_c)^p]$.

DOI: 10.1021/acs.iecr.6b02107
Ind. Eng. Chem. Res. 2016, 55, 9295−9311

$$v_x = \frac{\eta_0\dot{\gamma}_c^2}{2\rho g_x}\left\{\frac{Z_{\mathrm{R,m}}^{2/p}}{(1-Z_{\mathrm{R,m}})^{2/p}}\left\{\eta_c + (1-\eta_c)(1-Z_{\mathrm{R,m}})\left[2 - {}_2F_1\left(1, 1; \frac{2}{p}+1; Z_{\mathrm{R,m}}\right)\right]\right\} - \frac{Z_{\mathrm{R}}^{2/p}}{(1-Z_{\mathrm{R}})^{2/p}}\left\{\eta_c + (1-\eta_c)(1-Z_{\mathrm{R}})\left[2 - {}_2F_1\left(1, 1; \frac{2}{p}+1; Z_{\mathrm{R}}\right)\right]\right\}\right\} \quad (117)$$

$$Q = \frac{\dot{\gamma}_{\mathrm{m}}^3\eta_0^2}{(\rho g_x)^2}\left\{\frac{1}{3}(1-Z_{\mathrm{R,m}})^{3/p} \times F_1\left(\frac{3}{p}; \frac{3}{p}+1, -2; \frac{3}{p}+1; Z_{\mathrm{R,m}}, \eta_c Z_{\mathrm{R,m}}\right) - \frac{\eta_c p}{(3+p)}Z_{\mathrm{R,m}}(1-Z_{\mathrm{R,m}})^{3/p} \times F_1\left(\frac{3}{p}+1; \frac{3}{p}, -1; \frac{3}{p}+2; Z_{\mathrm{R,m}}, \eta_c Z_{\mathrm{R,m}}\right)\right\} \quad (118)$$

$$h^2 + \frac{1}{\dot{\gamma}_c^p}\left(\frac{x}{t}\right)^p h^{2-p} - \frac{\eta_0}{\rho g_x}\left(\frac{x}{t}\right) - \frac{\eta_\infty}{\rho g_x \dot{\gamma}_c^p}\left(\frac{x}{t}\right)^{p+1} h^{-p} = 0 \quad (119)$$

$$\frac{\langle h\rangle_x}{h} = 1 - \frac{(1-Z_{\mathrm{R,m}})^{3/p}}{(1-\eta_c Z_{\mathrm{R,m}})^2} \times \left\{\frac{1}{3}F_1\left(\frac{3}{p}; \frac{3}{p}+1, -2; \frac{3}{p}+1; Z_{\mathrm{R,m}}, \eta_c Z_{\mathrm{R,m}}\right) - \frac{\eta_c p}{(3+p)}Z_{\mathrm{R,m}}F_1\left(\frac{3}{p}+1; \frac{3}{p}, -1; \frac{3}{p}+2; Z_{\mathrm{R,m}}, \eta_c Z_{\mathrm{R,m}}\right)\right\} \quad (120)$$

3.4.9. Meter–Bird — $\eta = \eta_\infty + (\eta_0 - \eta_\infty)/[1 + (\tau/\tau_c)^p]$.

$$v_x = \frac{\tau_c^2}{2\rho g_x\eta_0}\left\{\frac{Z_{\mathrm{S,m}}^{2/p}}{(1-Z_{\mathrm{S,m}})^{2/p}} + \frac{2\eta_c}{(2+p)}\frac{Z_{\mathrm{S,m}}^{2/p+1}}{(1-\eta_c Z_{\mathrm{S,m}})^{2/p+1}}{}_2F_1\left[\frac{2}{p}+1, \frac{2}{p}+1; \frac{2}{p}+2; \frac{(1-\eta_c)Z_{\mathrm{S,m}}}{1-\eta_c Z_{\mathrm{S,m}}}\right] - \frac{Z_{\mathrm{S}}^{2/p}}{(1-Z_{\mathrm{S}})^{2/p}} - \frac{2\eta_c}{(2+p)}\frac{Z_{\mathrm{S}}^{2/p+1}}{(1-\eta_c Z_{\mathrm{S}})^{2/p+1}}{}_2F_1\left[\frac{2}{p}+1, \frac{2}{p}+1; \frac{2}{p}+2; \frac{(1-\eta_c)Z_{\mathrm{S}}}{1-\eta_c Z_{\mathrm{S}}}\right]\right\} \quad (121)$$

$$Q = \frac{\tau_{\mathrm{m}}^3}{3(\rho g_x)^2\eta_0}(1-Z_{\mathrm{S,m}})^{3/p} \times F_1\left(\frac{3}{p}; \frac{3}{p}+1, 1; \frac{3}{p}+1; Z_{\mathrm{S,m}}, \eta_c Z_{\mathrm{S,m}}\right) \quad (122)$$

$$h^p - \frac{\eta_\infty}{(\rho g_x)}\frac{x}{t}h^{p-2} + \left(\frac{\tau_c}{\mathrm{St}}\right)^p - \frac{\eta_0\tau_c^p}{(\rho g_x)^{1+p}}\frac{x}{t}h^{-2} = 0 \quad (123)$$

$$\frac{\langle h\rangle_x}{h} = 1 - \frac{1}{3}\frac{(1-\eta_c Z_{\mathrm{S,m}})}{(1-\eta_c)}\left\{1 - \frac{\eta_c(1-Z_{\mathrm{S,m}})}{(1-\eta_c Z_{\mathrm{S,m}})} \times {}_2F_1\left[1, 1; \frac{3}{p}+1; \frac{(1-\eta_c)Z_{\mathrm{S,m}}}{1-\eta_c Z_{\mathrm{S,m}}}\right]\right\} \quad (124)$$

3.4.10. Reiner–Philippoff — $\eta = \eta_\infty + (\eta_0 - \eta_\infty)/[1 + (\tau/\tau_c)^2]$.

$$v_x = \frac{\tau_c^2}{2\rho g_x\eta_0} \times \left\{\frac{Z_{\mathrm{S,m}}}{(1-Z_{\mathrm{S,m}})} + \frac{\eta_c}{(1-\eta_c)^2}\left[\frac{(1-\eta_c)Z_{\mathrm{S,m}}}{(1-Z_{\mathrm{S,m}})} + \ln\left(\frac{1-Z_{\mathrm{S,m}}}{1-\eta_c Z_{\mathrm{S,m}}}\right)\right] - \frac{Z_{\mathrm{S}}}{(1-Z_{\mathrm{S}})} - \frac{\eta_c}{(1-\eta_c)^2}\left[\frac{(1-\eta_c)Z_{\mathrm{S}}}{(1-Z_{\mathrm{S}})} + \ln\left(\frac{1-Z_{\mathrm{S}}}{1-\eta_c Z_{\mathrm{S}}}\right)\right]\right\} \quad (125)$$

$$Q = \frac{\tau_{\mathrm{m}}^3}{3(\rho g_x)^2\eta_0}(1-Z_{\mathrm{S,m}})^{3/2} \times F_1\left(\frac{3}{2}; \frac{3}{2}+1, 1; \frac{3}{2}+1; Z_{\mathrm{S,m}}, \eta_c Z_{\mathrm{S,m}}\right) \quad (126)$$

$$h = \sqrt{\frac{1}{2}\left[\frac{\eta_\infty}{\rho g_x}\frac{x}{t} - \left(\frac{\tau_c}{\rho g_x}\right)^2\right] + \sqrt{\frac{1}{4}\left[\frac{\eta_\infty}{\rho g_x}\frac{x}{t} - \left(\frac{\tau_c}{\rho g_x}\right)^2\right]^2 + \frac{\eta_0\tau_c^2}{(\rho g_x)^3}\frac{x}{t}}} \quad (127)$$

$$\frac{\langle h\rangle_x}{h} = 1 - \frac{1}{3}\frac{(1-\eta_c Z_{\mathrm{S,m}})}{(1-\eta_c)}\left\{1 - \frac{\eta_c(1-Z_{\mathrm{S,m}})}{(1-\eta_c Z_{\mathrm{S,m}})} \times {}_2F_1\left[1, 1; \frac{3}{2}+1; \frac{(1-\eta_c)Z_{\mathrm{S,m}}}{1-\eta_c Z_{\mathrm{S,m}}}\right]\right\} \quad (128)$$

3.4.11. Peek–Mclean–Williamson — $\eta = \eta_\infty + (\eta_0 - \eta_\infty)/[1 + (\tau/\tau_c)]$.

$$v_x = \frac{\tau_c^2}{2\rho g_x\eta_0}\left\{\frac{Z_{\mathrm{S,m}}^2}{(1-Z_{\mathrm{S,m}})^2} + \frac{2\eta_c}{3}\frac{Z_{\mathrm{S,m}}^3}{(1-\eta_c Z_{\mathrm{S,m}})^3} \times {}_2F_1\left[3, 3; 4; \frac{(1-\eta_c)Z_{\mathrm{S,m}}}{1-\eta_c Z_{\mathrm{S,m}}}\right] - \frac{Z_{\mathrm{S}}^2}{(1-Z_{\mathrm{S}})^2} - \frac{2\eta_c}{3}\frac{Z_{\mathrm{S}}^3}{(1-\eta_c Z_{\mathrm{S}})^3}{}_2F_1\left[3, 3; 4; \frac{(1-\eta_c)Z_{\mathrm{S}}}{1-\eta_c Z_{\mathrm{S}}}\right]\right\} \quad (129)$$

$$Q = \frac{\tau_{\mathrm{m}}^3}{3(\rho g_x)^2\eta_0}(1-Z_{\mathrm{S,m}})^3 F_1(3; 4, 1; 4; Z_{\mathrm{S,m}}, \eta_c Z_{\mathrm{S,m}}) \quad (130)$$

$$h^3 + \left(\frac{\tau_c}{\rho g_x}\right)h^2 - \frac{\eta_\infty}{\rho g_x}\frac{x}{t}h - \frac{\eta_0\tau_c}{(\rho g_x)^2}\frac{x}{t} = 0 \quad (131)$$

DOI: 10.1021/acs.iecr.6b02107
Ind. Eng. Chem. Res. 2016, 55, 9295−9311

$$\frac{\langle h\rangle_x}{h} = 1 - \frac{1}{3}\frac{(1-\eta_c Z_{S,m})}{(1-\eta_c)}\left\{1 - \frac{\eta_c(1-Z_{S,m})}{(1-\eta_c Z_{S,m})}\times {}_2F_1\left[1, 1; 4; \frac{(1-\eta_c)Z_{S,m}}{1-\eta_c Z_{S,m}}\right]\right\} \tag{132}$$

3.4.12. Ellis — $\eta = \eta_0/[1 + (\tau/\tau_c)^p]$.

$$v_x = \frac{\tau_c^2}{2\rho g_x \eta_0}\left\{\frac{Z_{S,m}^{2/p}}{(1-Z_{S,m})^{2/p+1}}\left[1 - \frac{p}{(2+p)}Z_{S,m}\right] - \frac{Z_S^{2/p}}{(1-Z_S)^{2/p+1}}\left[1 - \frac{p}{(2+p)}Z_S\right]\right\} \tag{133}$$

$$Q = \frac{\tau_m^3}{3(\rho g_x)^2\eta_0}\frac{[3 + p(1-Z_{S,m})]}{(3+p)(1-Z_{S,m})} \tag{134}$$

$$h^{2+p} + \left(\frac{\tau_c}{\rho g_x}\right)^p h^2 - \frac{\eta_0 \tau_c^p}{(\rho g_x)^{1+p}}\frac{x}{t} = 0 \tag{135}$$

$$\frac{\langle h\rangle_x}{h} = \frac{6 + (2 + Z_{S,m})p}{9 + 3p} \tag{136}$$

3.4.13. Newtonian.

$$v_x = \frac{\rho g_x h^2}{2\mu}\left[1 - \left(1 - \frac{y}{h}\right)^2\right] \tag{137}$$

$$Q = \frac{\rho g_x h^3}{3\mu} \tag{138}$$

$$h = \sqrt{\frac{\mu}{\rho g_x}\frac{x}{t}} \tag{139}$$

$$\frac{\langle h\rangle_x}{h} = \frac{2}{3} \tag{140}$$

4. CONCLUSIONS

In this work, an analytical and simple 2D mathematical model of the fluid-dynamic variables of the dip-coating draining stage of a finite vertical plate was developed. Concentrated dispersions were considered as film-forming fluids, whose rheological behavior was described by an extension of the theoretical rheological model proposed by Quemada.[16] The proposed model has been obtained based upon rigorous mass and momentum balances applied to the draining stage of a monophasic, isothermal, and nonevaporative system, where the highest forces are viscous and gravitational. The considered phenomena occur far away from the meniscus formed at the surface of the fluid-forming reservoir. Parameters that were estimated are the velocity profile (eqs 43–48 and 51–55), flow rate (eqs 60 and 64), average velocity (eqs 61 and 65), local thickness (eqs 69 and 70), and average thickness (eqs 73 and 75) of the film. Finally, the mathematical model was validated (prediction errors <15%) by using experimental data of average film thickness values of several representative concentrated dispersions obtained in this work and from the literature. These film-forming fluids were milk cream, condensed milk, 30% microparticulated whey protein suspension, food glaze suspension, milk chocolate, and deep-fat frying batters. The information published in this study can be useful to control and predict the homogeneity and thickness of the film during an industrial coating process, in order to decrease the trial-and-error predictions and satisfy the quality requirements of the final product.

■ AUTHOR INFORMATION

Corresponding Author

*Tel.: +54 342 451 1595; fax: +54 342 451 1079. E-mail address: jmperalta@intec.unl.edu.ar.

Notes

The authors declare no competing financial interest.

■ ACKNOWLEDGMENTS

This research was supported partially by Universidad Nacional del Litoral (projects CAI+D: 501 201101 00031 LI, 501 201101 00088 LI, and 501 201101 00156 LI) (Santa Fe, Argentina), Consejo Nacional de Investigaciones Científicas y Técnicas (Argentina), Agencia Nacional de Promoción Científica y Tecnológica (projects ANPCyT: 2011-182 and 2012-1413) (Argentina), and Secretaría de Estado de Ciencia, Tecnología e Innovación (project SECTEI: 2010-010-14) (Santa Fe, Argentina).

■ NOMENCLATURE

a_i = theoretical and experimental values of η or $\langle h\rangle_x$
C = concentration, kg m^{-3}
Ca = capillary number ($\eta U \sigma^{-1}$)
$\underline{e}_i$ = unit vector in the i^{th}-direction
$\underline{F}_e$ = external forces vector, N m^{-3}
$F_1[\alpha; \beta, \gamma; \delta; z_1, z_2]$ = Appell hypergeometric function
${}_2F_1[a, b; c; s]$ = Gauss hypergeometric function
Fr = Froude number ($U^2 g_x^{-1} h_L^{-1}$)
$\underline{g}$ = gravity acceleration vector, m s^{-2}
g = gravity acceleration component, m s^{-2}
h = local thickness of the film, m
h_L = h evaluated at L, m
L = length of the plate, m
N = number of data points in each studied suspension or number of studied suspensions
P = pressure, Pa
q, p = dimensionless coefficients used in eq 24
Q = flow rate per unit width, m^2 s^{-1}
Re = Reynolds number ($\rho U h_L \eta_{ref}^{-1}$)
St = Stokes number ($\rho g_x h_L^2 \eta_{ref}^{-1} U^{-1}$)
T = temperature, K
t = time, s
U = reference velocity for the x-direction, m s^{-1}
V = reference velocity for the y-direction, m s^{-1}
$\underline{v}$ = velocity vector, m s^{-1}
v = velocity component, m s^{-1}
$\underline{x}$ = position vector, m
x, y, z = Cartesian coordinates
Z_R = normalized and dimensionless shear rate parameter defined by eq 55
Z_S = normalized and dimensionless shear stress parameter defined by eq 47

Greek Symbols

Γ = dimensionless shear variable that could be $|\underline{\underline{\tau}}|/\tau_c$ or $|\underline{\underline{\dot\gamma}}|/\dot\gamma_c$
$\underline{\underline{\dot\gamma}}$ = rate-of-strain tensor, s^{-1}

DOI: 10.1021/acs.iecr.6b02107
Ind. Eng. Chem. Res. 2016, 55, 9295–9311

$|\underline{\underline{\dot{\gamma}}}|$ = magnitude of $\underline{\underline{\dot{\gamma}}}$, s^{-1}
$\dot{\gamma}_{ij}$ = rate-of-strain tensor component, s^{-1}
$\dot{\gamma}_c$ = characteristic shear rate, s^{-1}
ε = dimensionless ratio $(h_L L^{-1})$
η = apparent viscosity, Pa s
η_0 = limiting steady state viscosity when $\Gamma \to 0$ is used in eq 24, Pa s
η_∞ = limiting steady state viscosity when $\Gamma \to \infty$ is used in eq 24, Pa s
ρ = density, kg m^{-3}
σ = surface tension coefficient, N m^{-1}
$\underline{\underline{\tau}}$ = viscous stress tensor, Pa
$|\underline{\underline{\tau}}|$ = magnitude of $\underline{\underline{\tau}}$, Pa
τ_{ij} = viscous-stress tensor component acting in the j^{th}-direction on a plane with a normal vector acting in the i^{th}-direction, Pa
τ_c = characteristic shear stress used in eq 24, Pa

Subscripts

ref = reference state
x = in the x-direction
y = in the y-direction
z = in the z-direction

Special symbols

$\langle\rangle_i$ = averaged quantity in the i^{th}-direction
$\square$ = dimensionless quantity
$O()$ = "of the order of"

■ REFERENCES

(1) Grosso, D. How to Exploit the Full Potential of the Dip-Coating Process to Better Control Film Formation. *J. Mater. Chem.* **2011**, *21* (43), 17033.
(2) Kistler, S. F.; Schweizer, P. M. Coating Science and Technology: An Overview. In *Liquid Film Coating. Scientific principles and their technological implications*; Kistler, S. F., Schweizer, P. M., Eds.; Springer: Netherlands, Dordrecht, 1997; pp 3−15.
(3) Filali, A.; Khezzar, L.; Mitsoulis, E. Some Experiences with the Numerical Simulation of Newtonian and Bingham Fluids in Dip Coating. *Comput. Fluids* **2013**, *82*, 110.
(4) Schunk, P. R.; Hurd, A. J.; Brinker, C. J. Free-Meniscus Coating Processes. In *Liquid Film Coating. Scientific principles and their technological implications*; Kistler, S. F., Schweizer, P. M., Eds.; Springer: Netherlands, Dordrecht, 1997; pp 673−708.
(5) Tu, Y.; Drake, R. L. Heat and Mass Transfer during Evaporation in Coating Formation. *J. Colloid Interface Sci.* **1990**, *135* (2), 562.
(6) Brinker, C. J.; Hurd, A. J. Fundamentals of Sol-Gel Dip-Coating. *J. Phys. III* **1994**, *4* (7), 1231.
(7) Keeley, A. M.; Rennie, G. K.; Waters, N. D. Draining Thin films—Part 1. *J. Non-Newtonian Fluid Mech.* **1988**, *28* (2), 213.
(8) Pennington, S. V.; Waters, N. D.; Williams, E. W. The Numerical Simulation of an Oldroyd Liquid Draining down a Vertical Surface. *J. Non-Newtonian Fluid Mech.* **1990**, *34* (2), 221.
(9) Karnjanolarn, R.; Mccarthy, K. L. Rheology of Different Formulations of Milk Chocolate and the Effect on Coating Thickness. *J. Texture Stud.* **2006**, *37* (6), 668.
(10) Lee, S.; Ng, P. K. W.; Steffe, J. F. Effects of Controlled Mixing on the Rheological Properties of Deep-Fat Frying Batters at Different Percent Solids. *J. Food Process Eng.* **2002**, *25* (5), 381.
(11) Patel, B. K.; Bhattacharya, S. Coating with Honey: A Study with Model Solids. *J. Food Process Eng.* **2002**, *25* (3), 225.
(12) Agarwal, K.; Bhattacharya, S. Use of Soybean Isolate in Coated Foods: Simulation Study Employing Glass Balls and Substantiation with Extruded Products. *Int. J. Food Sci. Technol.* **2007**, *42* (6), 708.
(13) Eley, R. R.; Schwartz, L. W. Interaction of Rheology, Geometry, and Process in Coating Flow. *J. Coat. Technol.* **2002**, *74* (9), 43.
(14) Peralta, J. M.; Meza, B. E.; Zorrilla, S. E. Mathematical Modeling of a Dip-Coating Process Using a Generalized Newtonian Fluid. 1. Model Development. *Ind. Eng. Chem. Res.* **2014**, *53* (15), 6521.
(15) Peralta, J. M.; Meza, B. E.; Zorrilla, S. E. Mathematical Modeling of a Dip-Coating Process Using a Generalized Newtonian Fluid. 2. Model Validation and Sensitivity Analysis. *Ind. Eng. Chem. Res.* **2014**, *53* (15), 6533.
(16) Quemada, D. Rheological Modelling of Complex Fluids. I. The Concept of Effective Volume Fraction Revisited. *Eur. Phys. J.: Appl. Phys.* **1998**, *1* (1), 119.
(17) Berli, C. L. A.; Quemada, D. Rheological Modeling of Microgel Suspensions Involving Solid−Liquid Transition. *Langmuir* **2000**, *16* (21), 7968.
(18) Quemada, D.; Berli, C. Energy of Interaction in Colloids and Its Implications in Rheological Modeling. *Adv. Colloid Interface Sci.* **2002**, *98* (1), 51.
(19) Souliès, A.; Pruvost, J.; Legrand, J.; Castelain, C.; Burghelea, T. I. Rheological Properties of Suspensions of the Green Microalga Chlorella Vulgaris at Various Volume Fractions. *Rheol. Acta* **2013**, *52* (6), 589.
(20) Olivares, M. L.; Berli, C. L. A.; Zorrilla, S. E. Rheological Modelling of Dispersions of Casein Micelles Considered as Microgel Particles. *Colloids Surf., A* **2013**, *436*, 337.
(21) Pal, R. *Rheology of Particulate Dispersions and Composites*; Surfactant science series; CRC Press: Boca Raton, FL, 2007.
(22) Mohos, F. Á. Appendix 3: Survey of Fluid Models. In *Confectionery and Chocolate Engineering*; Wiley-Blackwell: Oxford, UK, 2010; pp 582−605.
(23) Casson, N. A. A Flow Equation for Pigment−Oil Suspensions of the Printing Ink Type. In *Rheology of Disperse Systems*; Mill, C. C., Ed.; Pergamon Press: London, 1959.
(24) Reiner, M. *Deformation, Strain and Flow: An Elementary Introduction to Rheology*, 3rd ed.; H. K. Lewis: London, 1969.
(25) Bird, R. B.; Hassager, O. *Dynamics of Polymeric Liquids I. Fluid Mechanics*, 2nd ed.; Wiley: New York, 1987; Vol. *1*.
(26) Papanastasiou, T. C.; Georgiou, G. C.; Alexandrou, A. N. *Viscous Fluid Flow*; CRC Press: Boca Raton, FL, 1999.
(27) Sisko, A. W. The Flow of Lubricating Greases. *Ind. Eng. Chem.* **1958**, *50* (12), 1789.
(28) Bingham, E. C. *Fluidity and Plasticity*; McGraw-Hill: 1922.
(29) Cross, M. M. Rheology of Non-Newtonian Fluids: A New Flow Equation for Pseudoplastic Systems. *J. Colloid Sci.* **1965**, *20* (5), 417.
(30) Meter, D. M.; Bird, R. B. Tube Flow of Non-Newtonian Polymer Solutions: PART I. Laminar Flow and Rheological Models. *AIChE J.* **1964**, *10* (6), 878.
(31) Peek, R. L.; McLean, D. A. Some Physical Concepts in Theories of Plastic Flow. *J. Rheol. (Easton, Pa.)* **1931**, *2* (4), 370.
(32) Srivastava, H. M.; Hussain, M. A. Fractional Integration of the H-Function of Several Variables. *Comput. Math. Appl.* **1995**, *30* (9), 73.
(33) Gutfinger, C.; Tallmadge, J. A. Films of Non-Newtonian Fluids Adhering to Flat Plates. *AIChE J.* **1965**, *11* (3), 403.
(34) Cisneros-Zevallos, L.; Krochta, J. M. Whey Protein Coatings for Fresh Fruits and Relative Humidity Effects. *J. Food Sci.* **2003**, *68* (1), 176.
(35) Meza, B. E.; Peralta, J. M.; Zorrilla, S. E. Rheological Properties of a Commercial Food Glaze Material and Their Effect on the Film Thickness Obtained by Dip Coating: Rheology of Food Glaze and Film Thickness. *J. Food Process Eng.* **2015**, *38* (5), 510.
(36) Schorsch, C.; Jones, M. G.; Norton, I. T. Thermodynamic Incompatibility and Microstructure of Milk Protein/locust Bean Gum/sucrose Systems. *Food Hydrocolloids* **1999**, *13* (2), 89.
(37) Odic, K. Rheology and Microstructure of Model Ice Cream Systems. Ph.D., University of Cambridge: Cambridge, UK, 2004.
(38) Weisstein, E. W. Appell function F1; http://functions.wolfram.com/HypergeometricFunctions/AppellF1/ (accessed Feb 24, 2016).

DOI: 10.1021/acs.iecr.6b02107
Ind. Eng. Chem. Res. 2016, 55, 9295−9311